UNIVERSITY OF THESSALY
SCHOOL OF ENGINEERING
DEPARTMENT OF MECHANICAL ENGINEERING

MODELLING OF BIOMASS COMBUSTION AND FLAME PROPAGATION IN WILDFIRES

by
ILIAS KALTSAS

Submitted in partial fulfillment of the requirements for the Master's degree in Analysis and Management of Energy Systems

Volos, 2025

ΠΑΝΕΠΙΣΤΗΜΙΟ ΘΕΣΣΑΛΙΑΣ
ΠΟΛΥΤΕΧΝΙΚΗ ΣΧΟΛΗ
ΤΜΗΜΑ ΜΗΧΑΝΟΛΟΓΩΝ ΜΗΧΑΝΙΚΩΝ

ΜΟΝΤΕΛΟΠΟΙΗΣΗ ΚΑΥΣΗΣ ΒΙΟΜΑΖΑΣ ΚΑΙ ΔΙΑΔΟΣΗΣ ΦΛΟΓΑΣ ΣΕ ΔΑΣΙΚΕΣ ΠΥΡΚΑΓΙΕΣ

υπό
ΗΛΙΑ ΚΑΛΤΣΑ

Υπεβλήθη για την εκπλήρωση μέρους των απαιτήσεων για
την απόκτηση του Μεταπτυχιακού Διπλώματος «Ανάλυση και Διαχείριση Ενεργειακών Συστημάτων»

Βόλος, 2025

Approved by the Committee on Final Examination:

Advisor	Dr. Vasilis Bontozoglou, Professor, Department of Mechanical Engineering, University of Thessaly
Member	Dr. Konstantinos Ampountolas, Professor, Department of Mechanical Engineering, University of Thessaly
Member	Dr. Costas Papadimitriou, Professor, Department of Mechanical Engineering, University of Thessaly

Date Approved:

MODELLING OF BIOMASS COMBUSTION AND FLAME PROPAGATION IN WILDFIRES

Ilias Kaltsas

Department of Mechanical Engineering, University of Thessaly

Supervisor: Dr Vasilis Bontozoglou

Professor

Abstract

The notable increase in extreme wildfire occurrence frequency observed in recent years and its adverse societal and environmental effects is a phenomenon that necessitates research aimed at understanding its underlying physical mechanisms, in order to develop effective methods of prediction and counteraction. To this end, models that can provide realistic estimations of a wildfire's rate of spread can be crucial in predicting how it will behave and what countermeasures may be employed to successfully suppress it. The aim of the current thesis is to enhance one such physical model's estimation of biomass combustion to inform its role in the wildfire's rate of spread.

The temperature evolution with time in a fuel particle's bulk, considered an infinite cylinder, during the flame front's passing, is modelled with a one-dimensional transient heat diffusion equation. It is implemented in a MATLAB code and approximated using a semi-implicit finite difference scheme, taking into account the temperature dependence of heat conductivity and steam and volatile generation, and the effect of natural convection and forced convection caused by volatile generation. The effect of the absence of steam generation, volatile generation or both, as well as the effect of initial moisture content and fuel particle radius in the temperature's distribution and the interrelation of the temperature dependent terms is then explored.

Key words: heat transfer, wildfire modelling, physical modelling, biomass combustion

Contents

LIST OF TABLES

LIST OF FIGURES

Chapter 1. Introduction

1.1 Motivation

Wildfires have always been a part of forest ecosystems, playing a role in soil regeneration, plant and animal habitat readaptation, and nutrient provision, but there is a very noticeable and concerning rise in their frequency and intensity in recent years that shouldn't be left unaddressed. Recent studies have found that both extreme wildfire frequency and magnitude have increased more than twofold globally in the past two decades (Cunningham et al. 2024). The last couple of years was a particularly intense wildfire period globally, with severe wildfires occurring in Australia, North Africa, South America and Canada, not to mention the greatest wildfire ever recorded in the EU afflicting the Evros area in Greece. The devastating effects of these wildfires are not only measured in the loss of human life, but also the extinction of entire unique ecosystems, the premature simultaneous release of massive quantities of greenhouse gases into the atmosphere and the destabilisation of local economies and property.

The correlation between this increase in the occurrence and intensity of wildfires and anthropogenic pressure on forests and climate change is notable. Population density and agricultural and industrial land use bordering with forests are major drivers of wildfire ignition, and modern urbanisation is the underlying cause of socioeconomic and topographical changes that also play a part in wildfire occurrences (Nunes et al. 2016). The meteorological effects brought about by climate change, in particular the latest interactions between droughts, temperature increase and novel wind phenomena and their combined lengthening effect on fire seasons seem to be another severe cause of extreme wildfires (Duane et al. 2021). Of special note is the increase in the vapour pressure deficit (VPD), the difference between water vapour pressure at saturation and the actual water vapour pressure for a given temperature, due to its effects on fuel content. A global increase in VPD due to climate change is causing a decrease in vegetation growth, as well as periodical shifts in fuel moisture contents due to

inhibition of plants' ability to regain moisture overnight, and so fuel is more abundant and more prone to ignition (Duane et al. 2021, Mueller et al. 2020).

The fact that wildfires are projected to increase in severity in the future due to the effects of climate change, along with the implications of this increase concerning environmental stability and human quality of life, invokes the need for research focused on all wildfire aspects, from methods of predicting, spotting and firefighting to models aimed at understanding the mechanisms associated with wildfire ignition and spread. Indeed, although wildfires have been a research subject for a long time now and wildfire models have been around since at least the 1940s (Naian et al. 2021), a great surge in wildfire research has been observed the past few years, integrating newer findings, technologies and concepts. Still, the very basis of the phenomenon and something humanity has lived with since its very early days, the combustion process, or simply fire itself, is not yet well understood (Rein, 2013). Thus, there is still need for further research on the mechanism of biomass combustion, the effects of fuel characteristics on it, and its interrelations with other fire spread parameters, in order to better simulate a wildfire's behaviour so as to inform our understanding and counteracting potential.

1.2 Problem Introduction

In this thesis, one such attempt of biomass combustion modelling, meant as an enhancement of an existing physical model's fuel combustion estimation meant to serve as the core of a broader wildfire prediction tool (Vogiatzoglou et al. 2024), is made. Its purpose is to serve as an adequate representation of fuel absorption of energy, volatile and steam generation in larger fuel particles. In such cases, the local temperature within the fuel's bulk plays a significant role in determining volatile and steam generation rates; first-order Arrhenius kinetics are too simple to accurately describe pyrolysis over wide temperature ranges (Saastamoinen and Richard, 1996). The approach here is to model fuel dehydration, pyrolysis, and combustion as overlapping heat transfer dominated processes with a fast rate of kinetics, and the whole problem as a one-dimensional heat diffusion one, with fuel particles modelled as infinite cylinders. This also allows for setting the basis of approximating the behaviour of flaming and non-flaming combustion, in the sense that volatile generation would be fuelling the buoyancy-driven flame, while the local temperatures at the fuel's bulk, maintained at high levels during and after the flame front's passing, would produce char that

could then be oxidized, if the material was porous enough, to continue glowing or smouldering combustion after the flame's passage (Sullivan, 2022).

The heat diffusion equation is implemented in a MATLAB code which uses a semi-implicit finite difference scheme to calculate the local temperature in the fuel particle's bulk. Temperature is calculated implicitly, but temperature-dependent terms such as volatile and steam generation, heat conductivity etc. are calculated at each time step. The results of a base scenario are then run against different assumptions on the presence of steam and/or volatiles, initial fuel moisture content and particle radius.

1.3 Thesis organization

The remainder of this thesis is structured as follows:

In **Chapter 2**, a literature review on wildfire research in general, wildfire modelling and biomass fuel combustion modelling in particular, is presented.

In **Chapter 3,** a focused review of the wildfire spreading model by Vogiatzoglou et al. is made, expanding on its enhancement potential by the modelling approach employed in the thesis.

In **Chapter 4,** the mathematical formulation of the problem and the methodology of its numerical approximation used in the code is detailed.

In **Chapter 5,** the results of the model runs and sensitivity analyses are presented and discussed.

Finally, **Chapter 6** includes a summary of the work done, concluding remarks and suggestions for further research.

Chapter 2. Literature Review

2.1 General Overview

Wildfire research is by necessity an intersectoral, multidisciplinary field. A recent bibliometric study, for example, concentrating and analysing almost 9000 scientific publications on forest fires, has classified them under the fields of Environmental Science (24.4 % of the published literature), Agricultural and Biological Sciences (17.9 %), Earth and Planetary Sciences (13.2 %), Engineering (10.5 %), Computer Science (10.2 %), Social Sciences (6.6 %), and Mathematics (4.5 %) (Bergali et al., 2024). Quantitative and qualitative analysis of fire behaviour, mechanisms, area of effect, occurrence probability etc. is a major focus, but the study of underlying causes, socioeconomic effects, necessity for countermeasures devising and funding, etc. is also a big part of the research.

One major area of interest concerns the factors contributing to the probability of a wildfire occurrence. A classification of these factors includes a) climatic factors, including variables such as temperature, humidity, wind speed and direction, evapotranspiration etc. b) topographic factors, such as ground slope, aspect, and altitude, c) in-situ factors, including fuel and soil characteristics d) historical incidents of occurrences and e) anthropogenic factors, including proximity to areas of human activity, roads, etc. (Mhawej et al., 2015). It is evident that of these variables, the climatic, topographic and in-situ factors, being quantifiable, are the most relevant to wildfire modelling, but the rest can also be incorporated in modelling processes such as statistical analysis.

Another aspect of research related to wildfire ignition but also fire behaviour in terms of severity is the fire danger rating systems and indices, which accumulate characteristic cause factors, most usually from the climatic, topographic and in-situ classes, and possible interrelations between them in order to estimate the danger of ignition or an ignition's effects. These are often used as sources of historical or real-time data to perform risk assessments. A plethora of systems and indices are used worldwide, with some of the most well known being the Canadian Forest Fire Danger Rate System (CFFDRS), especially one of its components, the Fire Weather Index (FWI), which comprises of modules related to fuel moisture, wind, and humidity, the National Fire Danger Rating System (NFDRS) in the USA, which uses interrelations between meteorological, fuel and topographical inputs to produce output indices related to combustion physics, fire behavior and fire danger severity, the BEHAVE system, which uses a similar approach with the NFDRS but more focused on fire behaviour

prediction instead of fire danger rating, the Angstrom Index in Sweden, based on relative humidity and temperature at 13:00 local time, and the Australian Forest Fire Danger Index (FFDI), based on a drought factor, relative humidity, temperature, and fuel characteristics (Zacharakis and Tsihrintzidis, 2023). Some of these incorporate physics-based, empirical, or statistical models in their calculations or are used themselves as the bases of models, as will be shown in the next section.

The environmental and socio-economic effects of wildfires is also a significant related research area. Forest fires may adversely affect biodiversity, wildlife habitats and ecosystem properties wherever they occur, and increasing frequency is more likely to have a worse impact. While forests act as carbon sinks, wildfires abruptly and prematurely turn them into carbon sources, amongst other emissions, and seem to form a closed loop with climate change, driving it as much as being driven by it (Kala, 2023). Another adverse effect of wildfires is the increase in subsequent flooding probability in areas burned and neighbouring ones, as wildfires may alter the hydraulic conductivity of the soil and thus very significantly increase the surface runoff (Sutanto et al., 2024). The socio-economic impact is also significant, as wildfires have devastating effects on entire settlements, rendering people homeless, destroying crops, resource pressure on their suppression, health hazards etc. (Roman et al., 2013, Kala, 2023).

For all these reasons, research aimed at understanding the mechanisms driving ignition risk, flame characteristics, rate of spread, fuel combustion, etc. is crucial in order to be able to counteract the adverse effects of wildfires. To this end, mathematical modelling of wildfires, comprising of a wide range of methodologies of numerically solving equations that describe the spatial and temporal evolution of wildfire variables, has been an ongoing subject matter since at least the 1940s. An overview of modelling methodologies and a more in-depth examination of some relevant models is presented in the next section.

2.2 Wildfire Modelling

The broader categorisation of wildfire models distinguishes them, based on the mathematical approach they employ, into three main types: a) statistical, models that do not attempt to involve physical mechanisms and only provide statistical descriptions of test fires and, as such, can be very successful in predicting similar fires to the test ones' behaviour; b) empirical, models that are based on energy conservation but make no distinction between different modes of heat transfer; and c) physical, models that do differentiate between modes

of heat transfer and attempt to approximate the wildfire related variables using more fundamental physical and mathematical means (Weber, 1991). To be able to further capture specific modelling aspects, wildfire models can be further classified according to the nature of the equations used, the variables calculated, and the physical system modelled (Pastor et al., 2003), as shown in the table below. Both classification methods are not exhaustive, and some models could fall under more than one categories, or wider model coupling approaches can be derived.

Table 2.1. Wildfire models classification (based on Pastor et al., 2003)

Classification basis	*Type*	*Description*
According to the nature of equations	Theoretical models	Generated from the laws governing fluid mechanics, combustion and heat transfer. Difficult to validate
	Empirical models	Generated using statistical correlations from experimental or historical wildfire data. Applicable only to very similar systems to the ones used on formulation
	Semi-empirical models	Based on simplified general and theoretical expressions and completed through experimentation. Applicable on situations similar to the ones used on formulation. Difficult to validate but less than the theoretical models.
According to the variables studied	Wildland fire spread models	Provide the mechanisms for calculating the main physical variables directly related to the fire perimeter advance: rate of spread, fire line intensity and fuel consumption.
	Fire front properties models	Describe flame characteristics like height, length, depth, and angle of inclination.
According to the physical system modelled	Surface fire models	The physical system is made of surface fuel less than 2 m high.
	Crown fire models	The physical system is made of surface fuel and aerial vegetation strata. If the fire front spreads at both strata simultaneously, there is an active crown fire. If the fire front consumes surface fuel and the crowns of individual trees, there is a passive crown fire.
	Spotting models	The physical system consists of firebrands or pieces of burning material which are transported by the convection column and carried beyond the main perimeter of the fire.
	Ground fire models	The physical system covers the organic forest horizons below the litter which are formed by fermentation and humus layers that accumulate above mineral soil.

Before proceeding to the next section examining some of the most known models, a mention of current approaches using Artificial Intelligence (AI) or Machine Learning (ML) algorithms is of worth, since it is a promising field with both standalone and coupling with physics-based models potential. One could argue that most AI/ML algorithms could be

thought of as statistics-based mathematical algorithms, and as such, standalone AI/ML models of wildfires essentially fall under the statistical category. Indeed, regardless of AI/ML approach used (regression, classification, decision trees/random forest, support vector machines, artificial neural networks etc.) they are data-centric methods, not concerned with the physical mechanisms of wildfires, whose performance depends on the quality of training data and its generalising potential (Jain et al., 2020). Their usage can be applied to a wide range of topics on wildfires, and they offer significant advantages in real-time calculations, while also able to be coupled with physical or empirical models, providing for example the otherwise user-defined input data and patterns in them, like meteorological conditions, spatial data retrieved by GIS or otherwise, local fuel characteristics etc. (Jain et al., 2020, Singh et al., 2024).

In the next section, some of the most well-known wildfire models of various methodologies and usages will be presented, attempting to highlight different aspects of wildfire modelling.

2.3 Models

Rothermel

The Rothermel model is one of the most well-known and used fire spread models, from its development by Richard C. Rothermel in 1972 until today. In its final form, improvements made by Frank A. Albini in 1976, made during its incorporation into a fire program named FIREMOD, have been integrated into the original model. The Rothermel model is a surface fire spread, semi-empirical model, which considers fire as a series of ignitions and its spread the rate at which potential fuel can be raised to ignition temperature. Its main equation is thus the ratio of the heat received by the potential fuel ahead of the fire front to the heat required for its ignition (Andrews, 2018):

$$R = \frac{I_R \xi (1 + \varphi_w + \varphi_s)}{p_b \varepsilon Q_{ig}} \qquad (eq. 2.3.1)$$

Where:

R: fire spread rate [m/min]

I_R: reaction intensity [kJ m/min m^2], the energy release rate per unit area of fire front

ξ: propagating flux ratio, the proportion of the reaction intensity that heats adjacent fuel particles to ignition

φ_w: wind factor

φ_s: slope factor

p_b: bulk density of fuel bed [kg/m^3]

ε: effective heating number, the proportion of a fuel particle that is heated to ignition temperature at the time flaming combustion starts

Q_{ig}: heat of preignition [kJ/kg], the amount of heat required for ignition of a fuel's unit of mass.

Parameters φ_w and φ_s depend on the packing ratio, which is the fraction of the fuel bed volume occupied by fuel, and the fuel particle's surface to volume ratio. The reaction intensity, which represents the heat released, does not differentiate between heat transfer modes.

The Rothermel model has been highly influential in the whole field of wildfire modelling, with several other models and programs incorporating it as is or trying to overcome its accuracy limitations (like for example high moisture fuel beds, according to Singh et al. 2024). Models that have at least at some point been based on the Rothermel model include BEHAVE/BehavePlus, FARSITE, FlamMap, CAWFE, and FireStem (Wells, 2008, Singh et al. 2024).

BEHAVE/BehavePlus

BehavePlus, the current updated version of the older wildfire prediction BEHAVE Fire Behavior Prediction and Fuel Modeling System first developed in 1976, is a modular system comprising of a collection of mathematical fire models, each related to a specific wildfire topic which can be used either autonomously or together, with outputs of one module being the inputs of another. It is one of the most commonly used fire modelling systems, covering almost all basic aspects of wildfire modelling. At its core is SURFACE, a surface fire spread module employing the Rothermel model with the relevant user defined inputs needed by it and calculating the surface fire rate of spread, the fireline and the reaction intensity. Other modules include a) CROWN, a module that calculates the transition from surface to crown fire, its spread, area and perimeter, and other characteristics b) SAFETY, which calculates the safe zone side based on flame height c) SIZE, calculating an elliptically shaped point source fire's length-to-width ratio and size d) CONTAIN, calculating given resources' probability of fire

containment success e) SPOT, calculating maximum spotting distance from torching trees, burning piles or wind-driven surface fire f) SCORCH, calculating crown scorch height from surface fire flame length g) MORTALITY, calculating the probability of mortality from bark thickness and crown scorch and h) IGNITE, calculating the probability of ignition by firebrands and/or lightning strikes (Andrews, 2013).

FIRETEC

FIRETEC was developed at the Los Alamos National Laboratory in the USA. It is a coupled multiphase transport-wildland fire physical model, based on the principles of conversation of mass, momentum and energy (Sullivan, 2009), although other researchers consider it semi-empirical (Singh et al. 2024). It is a fully three-dimensional representation of the coupled interactions of combustion, heat transfer, and fluid mechanics involved in wildland fire on a landscape scale. It is also coupled with a CFD model, HIGRAD, used for solving high gradient flow, such as the motions of the local atmosphere, and feeding the results as an input to FIRETEC (Bakhshaii, 2019, Sullivan, 2009). It utilizes the finite volume method, solving numerically its system of equations, attempting to represent the average behaviour of gases and solid fuels in a wildfire, while also incorporating simplified models for combustion reactions such as pyrolysis, char burning, hydrocarbon and soot combustion in the presence of oxygen, and although not suited for operational fire spread prediction and of limited scale and coupling capabilities, it has been proved very useful for research purposes in fire dynamics, fuel treatment effects, fire planning, rate of fire spread propagation and crown fire rate of spread (Bakhshaii, 2019, Sullivan, 2009). It is highly customisable but computationally intensive and as such not suited for real-time predictions (Singh et al. 2024).

Coupled Atmosphere-Wildland Fire Environment (CAWFE)

CAWFE is a coupled atmposphere-wildland fire-environment model developed at the National Centre for Atmopheric Research (NCAR) in the USA in 2004 as a first attempt to pair atmospheric and fire models (Singh et al. 2024). It employs basic thermodynamic and motion equation to simulate convective processes of a wide range, being able to capture prevailing meteorological conditions in three dimensions. In its current form, it includes a fire model behaviour module and a numerical weather forecast model. The fire model component incorporates the Rothermel fire spread rate formula and categorises fuel cells with tracers which indicate the burning regions of fuel and the fire front, where burning and unignited fuel

meet. The results are fed into the numerical model to affect meteorological conditions which affect the fire propagation, creating a coupling feedback loop. Despite its range, it currently is too computationally intensive to be used in real-time applications (Bakhshaii et al. 2019, Singh et al. 2024).

WRF-FIRE and WRF-SFIRE

The Weather Research Forecast (WRF) model is a fully operational numerical weather prediction (NWP) model used in a wide range of applications, like real-time forecast, research, coupled-model applications, regional climate research, and data assimilations. Its open-source license and modular framework allows it to both be operated and developed by thousands of scientists and to be coupled with models of wildfires with relative ease, combining its scaled physics, dynamic parameterization, employment of dynamic solvers, and data assimilation with the more focused physics of wildfires and allowing for a wide array of customisation options. The FIRE and SFIRE (surface fire) add-on packages allow it to be coupled with wildfire physics packages inspired by the CAWFE model, feeding it with meterorological calculations by the WRF model, with promising potential for real-time forecast for wildland fires (Bakhshaii et al. 2019, Singh et al. 2024).

2.4 Fuel Characteristics and Combustion Modelling

In wildfire modelling and especially rate of spread models, biomass combustion is a topic with crucial significance. Even considering fuel modelling just a predefined input set of fuel characteristics, like in the Rothermel model (Andrews, 2018), there remains a need to incorporate that input into the modelling process in a meaningful way. The fuel characteristics that need to be modelled depend on the representation resolution of the processes involved in fuel combustion. These include: a) *drying*, the initial endothermic process where fuel moisture content in the surface and bulk of the fuel evaporates b) *pyrolysis*, or more accurately *thermal degradation*, a set of mostly endothermic processes involving the transformation of dry wood into char (*char formation, charring*) and volatile gases or solids, called “tar”, in lower temperatures (*volatilisation*) and c) *oxidation* of the gas phase (flaming combustion) and the solid phase (*glowing* or *smouldering combustion*, depending on temperature rate of oxygen arrival at the reacting char surface) , the exothermic processes of

combustion (Sullivan, 2022). These processes may overlap, especially in larger particles, where local transient temperature varies significantly.

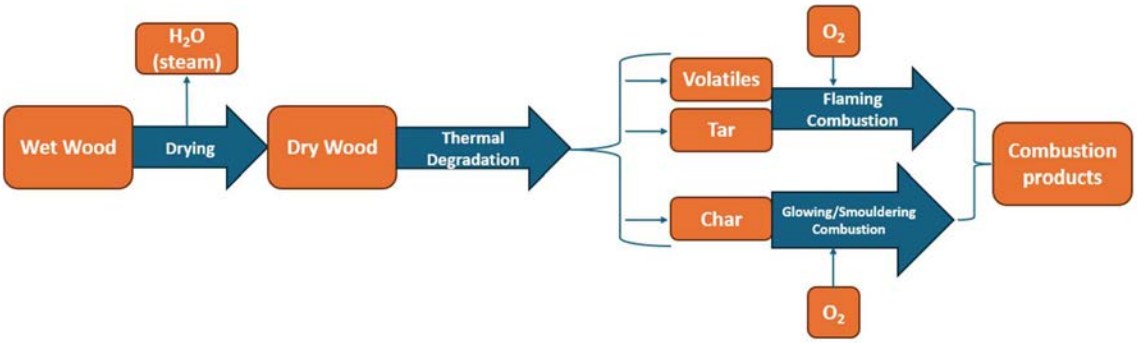

Fig.2.1. Simplified schematic diagram of the processes involved in biomass combustion

Ragland et al. (1991) have produced a categorisation of fuel properties useful for combustion modelling and analysis, grouping them under physical, thermal, chemical, and mineral. Some representative ones are presented in the table below.

Table 2.2. Fuel properties for combustion modelling

Physical	***Thermal***	***Chemical***	***Mineral***
density	wood specific heat	ultimate analysis	mineral content
bulk density	char specific heat	proximate analysis	ash yield
particle size	wood thermal conductivity	analysis of pyrolysis products	ash-fusion temperature
surface area per unit volume	char thermal conductivity	heating value of volatiles	
porosity	char emissivity	heating value of char	
char density		reaction rates	

Considering that this categorisation was made for the modelling of biomass combustion in controlled conditions, such as in boilers or wood stoves, elements particular in wildfire modelling are missing. A significant distinction in wildfire modelling, for example, is made in the Rothermel model between fuel particle properties (heat content, mineral content, particle density) and fuel bed properties (surface area to volume ratio, fuel load, depth, dead fuel moisture of extinction) (Andrews, 2018).

In the Rothermel model, a custom fuel model, consisting of the above properties and weighted averages of mixtures of dead and live fuel making up the fuel bed, is constructed using field data, running testing the model using them, and validating results comparing them to observed fire behaviour (Andrews, 2018). This is a procedure used by other models too, since modelling the fuel bed mixture of live and dead vegetation in forests is crucial in

determining the fuel load and the fuel moisture content, important parameters especially in the rate of spread calculation (McNorton and Giuseppe, 2024). Interestingly, although surface area to volume ratio (σ in the model) is important in the Rothermel model, its increase also increasing reaction intensity, propagating flux ratio, wind and slope coefficients, and effective heating number, which means both the heat source and the heat sink in equation (2.3.1) with the heat source dominating, particle size does not enter the model; it is just inferred in its relation to the surface area to volume ratio of the fuel bed.

A common approach in fuel combustion modelling concerning the processes involved in it, mainly pyrolysis and combustion, is to consider them temperature dependent kinetics-driven reactions, deriving their rate based on some variation or modification, accounting for fuel characteristics or other parameters related to the specific problem examined, of the first-order Arrhenius equation:

$$k = Ae^{-\frac{E_a}{RT}} \qquad (eq.\,2.4.1)$$

Where:

k: reaction rate

A: preexponential factor

E_a: molar activation energy

R: universal gas constant

T: absolute temperature

Either separate rates for each reaction and/or biomass component or a global rate expression can be used with varying degrees of efficiency (Ragland et al., 1991) and both methods are widely used in fuel modelling. For example, Mandel et al. (2008) formulate a physics-based wildland fire model which is based on a partial differential equation on conservation of energy, with an added term of fuel burning based on a global Arrhenius reaction. On the other hand, Porteiro et al. (2006) in their modelling of combustion of a single fuel particle use separate expressions based on first-order Arrhenius kinetics for the formation of volatiles, tar, and char by thermal degradation, and for the combustion of char.

There are disadvantages in using Arrhenius kinetics to describe pyrolysis (Saastamoinen and Richard, 1996). When it is used to derive volatile generation, the final yield

is not based on the local temperature at that specific instant, but on the fire layer's temperature, which may or may not be the actual local temperature. This problem becomes evident in larger fuel particles with wide variations of local intraparticle transient temperature. In these cases, volatile generation will probably be overestimated, as the local yield of char inside a particle is constrained by the asymptotic char-yield determined by the local temperature, which is expected to be lower the further from the fuel surface. Arrhenius kinetics assumes the existence of a constant final char yield at a final temperature, which is used to determine A and E, ignoring the local transient temperature effect. The Arrhenius temperature dependence also does not accurately represent fuels which have a wide pyrolysis temperature range, overestimating the rate at high temperatures and underestimating it at low ones. To overcome these problems, Saastamoinen and Richard (1996) model pyrolysis as a heat transfer dominated process, with the driving force behind it being the difference between the prevailing char density and the asymptotic yield $p_0 e(T)$, which they determine experimentally (see Chapter 4). Their model is then formulated as a PDE with right-side terms for the energy associated with pyrolysis and dehydration. Another approach could be that used by Leckner et al. (1999), who take into account a transition from a kinetic to a heat transfer regime, but Saastamoinen and Richard (1996) have found that a heat transfer dominated scheme is adequate.

In the next chapter, a presentation of an interpretable wildfire spreading model developed by Vogiatzoglou et al. (2024) with a focus on its fuel combustion modelling will be done, to set the basis for its potential enhancement on the basis of the approach of Saastamoinen and Richard (1996).

Chapter 3. The Wildfire Spreading Model

3.1 General Description of the Model

The model developed by Vogiatzoglou et al. is a physics-based, wildfire spread model, aiming to have a satisfactory approximation of the physics involved while remaining simple, interpretable, and not computationally intensive, which would pinpoint it at an intermediate point between oversimplified empirical models and advanced but computationally expensive CFD tools. This approach would enable its usage for real-time estimations, as it is intended to be used in the future as the basis of a wider decision tool for ongoing fires, coupled with processes feeding it remote sensing data at a continuous rate, recalibrating the model parameters accordingly and improving its accuracy.

By employing simplified forms of physical mechanisms influencing the rate of spread, the model produces a system of differential equations describing the spatiotemporal evolution of the two-dimensional fields of temperature and combustibles, accounting for variables such as the effect of mean wind velocity through the plantation and slope. The main heat transfer mechanisms included are: a) reaction kinetics for steam generation and wood combustion, represented by first-order Arrhenius rates b) heat transfer by convection from the gaseous phase's motion through the plantation, represented by a simple fluid dynamic argument, predicting the mean air velocity through the plantation c) heat transfer around the flame by turbulent transport and radiation, represented by a an effective dispersion coefficient which increases linearly with the mean wind velocity through the plantation and d) heat losses by free convection and radiation. The main equations of the model are the following:

$$\frac{\partial T}{\partial t} = \frac{c_1}{c_0}\left(\mathcal{D}_{eff,x}\frac{\partial^2 T}{\partial x^2} + \mathcal{D}_{eff,y}\frac{\partial^2 T}{\partial y^2} - \langle u_{eff,x}\rangle\frac{\partial T}{\partial x} - \langle u_{eff,y}\rangle\frac{\partial T}{\partial y}\right) - \frac{c_2}{c_0}S_1 r_1 + \frac{c_3}{c_0}S_2 r_{2t} - \frac{c_4}{c_0}U(T - T_a) \qquad eq.\,3.1.1$$

$$\frac{\partial S_1}{\partial t} = -S_1 r_1 \qquad eq.\,3.1.2$$

$$\frac{\partial S_2}{\partial t} = -S_2 r_{2t} \qquad eq.\,3.1.3$$

Where:

T: temperature [K]

t: time (s)

c_i: combinations of thermophysical properties calculated internally in the model

$\mathcal{D}_{eff,x-y}$: the dispersion coefficient vectors in each dimension, quantifying short range heat transport by radiation, buoyant instabilities and turbulent eddies. Proportional to the product of local velocity and length scales (distance from maximum field temperature), which are in turn subject to the effect of the wind [m^2/s]

$\langle u_{eff,x-y} \rangle$: the effective wind speed, obtained by the combination of the wind speed through the plantation with the local upstream component of the buoyant velocity of the thermal plume [m/s]

S_1: the dimensionless remaining fuel mass fraction of water ($S_1 = \frac{m_{s1}}{m_{s0}}$, where m_{s0} is the fuel bulk density of solid material [kg/m^3])

S_2: the dimensionless remaining fuel mass fraction of combustibles ($S_2 = \frac{m_{s2}}{m_{s0}}$)

U: an overall heat transfer coefficient for thermal losses to the environment [W/m^2K]

T_a: the ambient temperature [K]

In the right side of equation 3.1.1., the first two terms account for the effect of dispersion, quantifying radiative and convective short range heat transfer. The next two terms are the advection terms, incorporating the effect of wind speed through the plantation as well as the ground's inclination, included by means of the angle of the wind's direction with the upslope direction. The following terms describe the energy associated with the reactions, with the first representing the endothermic phase (wood dehydration) and the second the exothermic phase (thermal degradation and combustion). The final term represents heat losses to the environment. Each term has several subroutines running to determine its components before its insertion in the temperature calculation but a higher-resolution description of them is outside the scope of this overview. It is finally evident that equations 3.1.2 and 3.1.3 represent the temporal variations of water content and combustibles

Equations 3.1.1, 3.1.2 and 3.1.3 are discretised and approached by an explicit finite difference numerical scheme. The advection terms are approached by first-order upwinding

and the dispersion terms by second-order central differences, and the resulting ODE system is solved by Adams-Bashforth, utilising a suitable time step for stability of both.

As the temperature is calculated at each timestep, the firelength $\mathbf{w} = (w_x, w_y)$ is derived from the distribution of maximum temperatures in one dimension and their variation at the other, $T_{\max}(x_i, y_i)$, marking its endpoints $(x_A, y_A), (x_B, y_B)$ as the points for which $T_{max} > 550\ K$, which is the temperature where the exothermic phase is supposed to begin. Thus:

$$w_x = |x_A - x_B|$$
$$w_y = |y_A - y_B|$$

The progression of the firefront over time is derived from each calculation at each time step. The rate of spread can then be calculated from the displacement of the temperature maximum and the corresponding time lag. After running 1-D and 2-D simulations, the authors conclude that for all cases, the ROS is accurately described by the following equation:

$$\mathrm{ROS} = \lambda_1(1 - e^{-\lambda_2 w})$$

Where:

λ_1: the asymptotic velocity of the combustion wave for a long fireline (ROS_∞), mainly influenced by the wind velocity [m/s]

λ_2: a coefficient influencing the length w_0 of the fireline beyond which the asymptotic value ROS_∞ is reached [m^{-1}]

In the next section, a focus on equations 3.1.2 and 3.1.3, modelling the temporal variations of water and combustibles and the modelling enhancement potential of approaching them in a different manner will be explored.

3.2 Model Enhancement Potential

The main part of the fuel combustion modelling part of this wildfire spreading model occurs exactly at equations 3.1.2 and 3.1.3. A revisit in more detail could make some disadvantages in their approach more evident. First of all, the reaction rate for equation 3.1.2 is produced with the following calculation, following first-order Arrhenius kinetics:

$$r_1 = c_{s1} e^{-\frac{b_1}{T}} \qquad eq.3.2.1$$

Where:

c_{s1}, b_1: parameters quantifying differences in behaviour between dead and live moisture content ([s^{-1}] and [K] respectively)

T: temperature of the fire layer [K]

The reaction rate r_2 for the temporal variation of combustibles and as such the burning process is derived from an identical expression with different parameters, but in this case another inhibitor to the reaction rate is the amount of oxygen arriving at the spot for oxidation, so the total reaction rate takes these two inhibitions as resistances in series and is calculated as follows:

$$r_2 = c_{s2} e^{-\frac{b_2}{T}} \qquad eq.3.2.2$$

$$r_{2t} = \frac{r_2 r_m}{r_2 + r_m} = \frac{c_{s2} e^{-\frac{b_2}{T}} r_m}{c_{s2} e^{-\frac{b_2}{T}} + r_m} \qquad eq.3.2.3$$

Where:

c_{s2}, b_2: parameters depending on fuel characteristics, determining the intensity of pyrolysis and combustion ([s^{-1}] and [K] respectively)

r_m: rate of oxygen arrival to the burning solid [s^{-1}]

Parameters such as the fuel's size are taken into account only in the determination of the parameters determining pyrolysis intensity. The endothermic and exothermic phase are modelled as essentially taking place sequentially, as the Arrhenius-determined rates are dependent on the temperature and dehydration occurs at under 500 K while the reactions of pyrolysis and combustion begin at over 550 K.

Since this modelling approach does not take into account the variations of local temperature in the fuel's bulk, an inherent disadvantage of modelling combustion using Arrhenius kinetics as previously discussed, it is probable that volatile generation will be overestimated in larger particles, since it would be calculated based on the fire layer's

temperature instead of the actual local temperature, which may or may not be close to it. This also means that the interplay of steam and volatile generation is practically neglected. In order for this to be taken into account, the possibility of variations of temperature within the fuel's bulk enabling these processes to occur simultaneously in different parts of the fuel, where parts of it might be at the dehydration temperature zone and other parts at the pyrolysis temperature zones, and not consecutively assuming a uniform fuel temperature, needs to be considered.

To overcome these limitations, the problem can be reformulated by substituting the approximation of dehydration and combustion using Arrhenius kinetics with a heat diffusion model from the fuel's surface to its bulk, such that the temperature is a function of both time and spatial position within the particle ($T(r,t)$). This would also allow for a more accurate representation of fuel characteristics which are temperature dependent, such as heat conductivity and specific heat capacity of the fuel, while also covering the effect of local transient temperature in the generation of steam and volatiles. This transient temperature is also a good indicator of smouldering or glowing combustion within the fuel's bulk, while volatiles flowing through the bulk oxidise when reaching the surface, resulting in flaming combustion. The resulted calculations could then be fed back into equation 3.1.1, allowing for experimentation on the effect of fuel particle size, initial moisture content etc and their effect on the final rate of spread.

In the following chapter, one such attempt at modelling the problem of dehydration, pyrolysis and combustion is presented, detailing its mathematical formulation as well as the numerical approach for solving it in the MATLAB environment.

Chapter 4. Modelling Approach

4.1 Mathematical Formulation

The fuel has been modelled as a homogenous and porous, infinite horizontal cylinder, with the same initial assumptions on composition, specific heat capacity and other properties as suggested by Saastamoinen and Richard and shown in Table 4.2. The thermal energy balance through the fuel's bulk is modelled as:

$$pc(T)\frac{\partial T}{\partial t} = \frac{1}{r}\frac{\partial}{\partial r}\left(\lambda(T) r \frac{\partial T}{\partial r}\right) + l_p \dot{p_p} + l_w \dot{p}_w \qquad (eq.\ 4.1.1)$$

Where:

p: fuel density [kg/m^3]

c: specific heat capacity [J/kgK]

T: temperature [K]

t: time [s]

r: particle radius [m]

λ: wood heat conductivity [W/mK]

l_p: heat of decomposition [J/kg]

$\dot{p_p}$: local rate of volatile generation [kg/s m^3]

l_w: heat of decomposition [J/kg]

$\dot{p}_w$: local rate of steam generation [kg/s m^3]

In the above equation, the left side term accounts for heat storage, while the first term on the right side accounts for conduction and radiation heat transfer within the fuel's bulk, the second term represents the energy of the pyrolysis process and the third term represents the energy of the moisture evaporation process. The particle is assumed to shrink in density with volatile and steam generation under constant volume. The effect of moisture transfer as liquid water inside the particle is neglected, as is the convective cooling effect of the flow of volatiles and steam (Saastamoinen and Richard, 1996).

Fuel density (p), specific heat capacity (c), wood heat conductivity (λ) and the local rates of volatile and steam generation ($\dot{p_p}$, $\dot{p}_w$) are modelled as dependent on local transient

temperature, to better capture both their relation to temperature evolution as well as variations dependent on spatial allocation and as such, a better estimation of larger particle behaviour.

The local particle density is modelled using the following equations:

$$p = p_0 e(T) \qquad (eq.4.1.2)$$

$$e(T) = \begin{cases} \left(1 - 0.85 \exp\left[-\frac{9400}{(T - T_p)^2}\right]\right), & T > T_P \\ 1, & T \leq T_p \end{cases} \qquad (eq.4.1.3)$$

Where:

p_0: initial fuel density [kg/m^3]

$e(T)$: empirical function of temperature, developed by Saastamoinen and Richard (1996), using their own measurements on willow and fir combustion experiments

T_p: the temperature of pyrolysis initialisation, assumed to be 490 K.

Accordingly, the local rate of volatile generation is modelled as:

$$\dot{p_p} = -p_0 \mathrm{e}'(T) \frac{\partial T}{\partial t} \qquad (eq.4.1.4)$$

$$\mathrm{e}'(T) = \begin{cases} \frac{15980}{(T - T_p)^3} \exp\left[-\frac{9400}{(T - T_p)^2}\right], & T > T_p \\ 0, & T \leq T_p \end{cases} \qquad (eq.4.1.5)$$

The generation of steam is modelled as follows:

$$\dot{p}_w = -p_0 u_0 \mathrm{e}'_{wat}(T) \frac{\partial T}{\partial t} \qquad (eq.4.1.6)$$

$$e'_{wat}(T) = \begin{cases} 0.5\left(1 - \tanh(T - T_{vap})^2\right), & T > T_{vap} \\ 0, & T \leq T_{vap} \end{cases} \qquad (eq.4.1.7)$$

Where:

u_0: initial moisture content (%)

$e'_{wat}(T)$: empirical function of temperature, own assumption

T_{vap}: vaporization temperature, 373 K.

The fuel's specific heat capacity and heat conductivity have been assumed to vary linearly with temperature for simplicity. The allowed values vary between assumptions on the initial and final conductivity and specific heat capacity of wet wood and char. The variation starts when the local temperature reaches the temperature of water evaporation and ends when it reaches the temperature where pyrolysis ends.

$$\lambda(T) = \begin{cases} \lambda_w + \left(T - T_{vap}\right)\dfrac{(\lambda_{cha} - \lambda_w)}{T_{pend} - T_{vapstart}}, & T_{vap} \le T \le T_{pend} \\ \lambda_w, & T \le T_{vap} \\ \lambda_{char}, & T \ge T_{pend} \end{cases} \qquad (eq.\,4.1.8)$$

$$c(T) = \begin{cases} c_w + \left(T - T_{vap}\right)\dfrac{(c_{char} - c_w)}{T_{pend} - T_{vap}}, & T_{vap} \le T \le T_{pend} \\ c_w, & T \le T_{vap} \\ c_{char}, & T \ge T_{pend} \end{cases} \qquad (eq.\,4.1.9)$$

Where:

λ_w: initial heat conductivity of wood (wet) [W/mK]

λ_{char}: final heat conductivity of char [W/mK]

T_{pyend}: temperature of pyrolysis end (assumed to be 825 K)

c_w: initial specific heat capacity of wood (wet) [W/mK]

c_{char}: final specific heat capacity of char [W/mK]

Replacing the relevant terms of equation (4.1.1) with the equations (4.1.2), (4.1.4) and (4.1.6) and rearranging produces the following form of the energy balance:

$$p_0\left(c(T)e(T) + l_p e'(T) + l_w \mathrm{e}'_{wat}(T)\right)\frac{\partial T}{\partial t} = \frac{1}{r}\frac{\partial}{\partial r}\left(r\lambda(T)\frac{\partial T}{\partial r}\right)$$

The terms on the left side can then be assigned to a single temperature-dependent term, associated with heat storage, and named $H(T)$. The final form of equation (4.1.1) would then be:

$$H(T)\frac{\partial T}{\partial t} = \frac{1}{r}\frac{\partial}{\partial r}\left(r\lambda(T)\frac{\partial T}{\partial r}\right) \qquad (eq.4.1.10)$$

The boundary condition on the cylinder's surface, which in itself is the main driver of the whole heat transfer problem, is dictated by the passing of the flame profile. The following formulation expresses what the temperature profile of the surface would be, if no convection was taken into account. It represents a temperature spike of Gaussian shape, following Vogiatzoglou et al.:

$$T_{surface} = T_0(R) + (T_{max}(R) - T_0(R))\exp\left(-\frac{\sigma^2}{2}\right)\frac{1}{\tau}\exp\left[-\frac{1}{2}\left(\frac{\ln(\tau)}{\sigma}\right)^2\right] \qquad (eq.4.1.11)$$

$$\tau = \frac{t}{t_{max}} * \tau_{end} \qquad (eq.4.1.12)$$

Where:

R: the cylinder's radius [m]

T_{max}: assumption of the flame's maximum temperature [K]

σ: a constant number used to determine the temperature distribution's skewness, assumed to be 0.5

τ: the time dimension of the flame profile, mapped to the time dimension of the model through eq. 4.1.12

t_{max}: total simulation time

τ_{end}: the time at which the flame profile has passed.

A combined natural and forced convection heat transfer coefficient has been taken into account in the final calculation of the surface temperature. The air's density is calculated relatively to the cylinder surface's temperature. Assuming that the whole of the volatiles and steam generated at each time step immediately appears at the particle's surface and is immediately removed at the next time step, the working fluid of the convection is assumed to

have under constant volume the combined density of the three main gases in the mixture, air, volatiles (represented by carbon monoxide, CO) and steam, at each time step. The dynamic viscosity and thermal conductivity of each of the three gases is assumed to vary linearly with temperature, between their respective values in the initial and the maximum surface temperature. The dynamic viscosity and thermal conductivity of the gas mixture is then calculated as the weighted average of each gas' relevant value, with the weights being their individual contribution to the total gas mixture's density. The final gas mixture's buoyancy velocity, being the driver of the forced convection mechanism, is assumed to follow the flame's intensity, reaching its maximum simultaneously with the surface temperature. Under these assumptions, the equations used for forced and natural convection following Cengel, 2002 are as follows.

Forced Convection

$$Re = \frac{p_{mix} u D}{\mu_{mix}} \qquad (eq.4.1.13)$$

$$Nu_f = CRe^m Pr^{\frac{1}{3}} \qquad (eq.4.1.14)$$

Natural Convection

$$Gr = \frac{g\beta(T(R) - T_\infty)2R^3}{\nu^2} \qquad (eq.4.1.15)$$

$$Ra = GrPr \qquad (eq.4.1.16)$$

$$Nu_n = \left\{ 0.6 + \frac{0.387 Ra^{\frac{1}{4}}}{\left[1 + \left(\frac{0.559}{\mathrm{Pr}}\right)^{\frac{9}{16}}\right]^{\frac{4}{9}}} \right\}^2 \qquad (eq.4.1.17)$$

Combined Forced and Natural Convection

$$Nu = \left(Nu_f^4 + Nu_n^4\right)^{\frac{1}{4}} \qquad (eq.4.1.18)$$

$$h = \frac{Nuk_{mix}}{2R} \qquad (eq.4.1.19)$$

Where:

Re: Raynolds number of the gas mixture

p_{mix}: gas mixture density [kg/m^3]

u: buoyancy velocity [m/s]

D: particle diameter [m]

μ_{mix}: dynamic viscosity of the gas mixture [kg/ms]

Nu_f: Nusselt Number of forced convection

C, m: constants depending on Raynolds number range

Pr: Prandlt number (assumed constant)

Gr: Grashof number

g: gravitational acceleration [m/s^2]

T_∞: ambient temperature (considered same as cylinder initial temperature) [K]

v: kinematic viscosity

Ra: Rayleigh number

Nu_n: Nusselt number of natural convection

Nu: Nusselt number of combined forced and natural convection

h: convective heat transfer coefficient [W/m^{2}K]

Table 4.1. Values of C and m relative to the Reynolds number range (Cengel, 2002)

Re	*C*	*m*
0.4 - 4	0.989	0.330
4 - 40	0.911	0.385
40 - 4,000	0.683	0.466
4,000 - 40,000	0.193	0.618
40,000 - 400,000	0.027	0.805

4.2 Methodology

A MATLAB code implementing the mathematical formulation above and using it to numerically solve the equation (4.1.10) has been developed, tested and run under different scenarios of input data, considerations and sensitivity analyses.

A discretisation of the space between the particle's center and its surface and the simulation time is first employed in the following way:

$$r_i = i\Delta r, \qquad i = 1,2,\dots,N$$
$$t_n = n\Delta t, \qquad n = 1,2,\dots,M$$
$$\Delta r = \frac{R}{N\ -\ 1}$$
$$\Delta t = \frac{t_{max}}{M-1}$$

Where:

r_i: the current radial step

t_n: the current time step

Δr: radial step size

Δt: time step size

N: number of radial steps

M: number of time steps.

This allows the one-dimensional transient heat diffusivity problem represented by equation (4.1.10) to be approached by the finite difference method, based on Özisik et al. (2017) and Becker, Kaus (2020). The equation is discretised in the following way:

$$H(T_i^n)\frac{T_i^{n+1}-T_i^n}{\Delta t} = \frac{1}{r_i}\frac{\left(\lambda_{i+\frac{1}{2}}r_{i+\frac{1}{2}}\right)(T_{i+1}^{n+1}-T_i^{n+1})\ -\ \left(\lambda_{i-\frac{1}{2}}r_{i-\frac{1}{2}}\right)(T_i^{n+1}-T_{i-1}^{n+1})}{\Delta r^2} \qquad eq.(4.2.1)$$

Here, the use of i denotes grid points, while the use of $i \pm 1/2$ denotes grid point boundaries, which in the context of a horizontal cylinder are the centers of radius slices.
Rearranging equation 4.2.1:

$$-\frac{\Delta t}{H(T_i^n)r_i\Delta r^2}\left(\lambda_{i+\frac{1}{2}}r_{i+\frac{1}{2}}\right)T_{i+1}^{n+1}$$
$$+\left[1+\frac{\Delta t}{H(T_i^n)r_i\Delta r^2}\left(\lambda_{i+\frac{1}{2}}r_{i+\frac{1}{2}}+\lambda_{i-\frac{1}{2}}r_{i-\frac{1}{2}}\right)\right]T_i^{n+1}$$
$$-\frac{\Delta t}{H(T_i^n)r_i\Delta r^2}\left(\lambda_{i-\frac{1}{2}}r_{i-\frac{1}{2}}\right)T_{i-1}^{n+1} = T_i^n \qquad eq.(4.2.2)$$

This formulation can then be written in matrix form and solved as a system of linear equations:

$$A\mathbf{x} = \mathbf{b} \qquad (\text{eq. } 4.2.3)$$

Where:

A: the coefficient matrix

$\mathbf{x}$: the vector of left-side, unknown temperatures of eq. (4.2.2)

$\mathbf{b}$: the vector of right-side, known temperatures of eq. (4.2.2).

Specifically, the coefficient matrix and the temperature vectors are formed as follows:

$$A_{i,i+1} = -\frac{\Delta t}{H(T_i^n) r_i \Delta r^2}\left(\lambda_{i+\frac{1}{2}} r_{i+\frac{1}{2}}\right)$$

$$A_{i,i} = 1 + \frac{\Delta t}{H(T_i^n) r_i \Delta r^2}\left(\lambda_{i+\frac{1}{2}} r_{i+\frac{1}{2}} + \lambda_{i-\frac{1}{2}} r_{i-\frac{1}{2}}\right)$$

$$A_{i,i-1} = -\frac{\Delta t}{H(T_i^n) r_i \Delta r^2}\left(\lambda_{i-\frac{1}{2}} r_{i-\frac{1}{2}}\right)$$

$$\mathbf{x} = \begin{bmatrix} T_1^{n+1} \\ T_2^{n+1} \\ \vdots \\ T_i^{n+1} \\ \vdots \\ T_N^{n+1} \end{bmatrix}$$

$$\mathbf{b} = \begin{bmatrix} T_1^{n} \\ T_2^{n} \\ \vdots \\ T_i^{n} \\ \vdots \\ T_N^{n} \end{bmatrix}$$

T_1^n and T_N^n are determined by the following boundary conditions:

Boundary Condition at the Cylinder's Center (i = 1, r = 0 : $\Delta r/2$)

$$\left.\frac{\partial T}{\partial r}\right|_{r=0} = 0$$

$$H_1 \frac{T_1^{n+1} - T_1^n}{\Delta t} = \frac{4}{r_{3/2}} \frac{\left(\lambda_{3/2} r_{3/2}\right)(T_2^{n+1} - T_1^{n+1})}{\Delta r^2} \qquad (eq. 4.2.4)$$

Here, $r_{3/2}$ represents the boundary between the first and second radial point (that is, $i + \frac{1}{2}$ for $i = 1$).

Boundary Condition at the Cylinder's Surface (i = N, r = R − Δr/2 : R)

$$H_N \frac{T_N^{n+1} - T_N^n}{\Delta t} = h \frac{2}{\Delta r}(T_\infty - T_N^{n+1}) - \frac{2}{R} \frac{\left(\lambda_{N-\frac{1}{2}} r_{N-\frac{1}{2}}\right)(T_N^{n+1} - T_{N-1}^{n+1})}{\Delta r^2} \qquad (eq. 4.2.5)$$

Where $T_N = T_{surface}$.

Applying this condition to the boundary between the surface node and the previous node ($R - \Delta r/2$) calculates the surface temperature in relation to both the flame profile and the heat convection term.

Finally, after solving for the unknown temperature vector, volatile and steam generation is calculated for the whole of the fuel's bulk at each time step, as follows:

$$\dot{m}_v = \sum_{i=1}^{N} (-\dot{p_p}(T_i^{n+1} - T_i^n) 2\pi r_i \Delta r)$$
$$\dot{m}_{st} = \sum_{i=1}^{N} (-\dot{p_w}(T_i^{n+1} - T_i^n) 2\pi r_i \Delta r)$$

Where:

$\dot{m}_v$: volatile mass flow (kg/s)

$\dot{m}_{st}$: steam mass flow (kg/s).

The MATLAB code uses the above mathematical formulation to solve for x, effectively solving the entire system of equations simultaneously. This means that the temperature is calculated using the *implicit finite difference method.* This, however, is not the case for the temperature dependent terms, collected in the term $H(T)$. These terms are calculated using the known temperature T_i^n at each time step; as such, the general method employed is a

semi-implicit scheme. This limits the amount of time steps that produce non-oscillating results and is a disadvantage of the current modelling approach, as will be shown in the next chapter.

The model comprises of a routine which introduces the main input data used (shown in the table below), the initialisation of vectors and matrixes used and the functions that determine the temperature dependent terms. Four scripts can then be run either separately or one after another. These are:

- The *base* scenario, serving as reference to the rest.
- The *main* sensitivity analysis scenario which comprises of four subscripts called in order: a variation of the base scenario where steam generation is not taken into account, one where volatile generation is not taken into account and one where neither is. The fourth subscript reruns the base scenario and performs comparisons between it and the other three.
- The *moisture sensitivity analysis* scenario, where the effect of the wood's initial moisture content on temperature, steam and volatile generation is explored.
- The *radius sensitivity analysis* scenario, where the effect of radius on temperature, steam and volatile generation is explored.

The running time of a full run, using the input data of Table 4.2, was clocked at 50.573 s, running on an 11th Gen Intel(R) Core(TM) i5-1135G7 @ 2.40GHz. 26,2 seconds of this time were used to generate and store the graphs, meaning that the model run accounts for less than 25 seconds. The running time of just the base model run, excluding graph generation and storage, is at just 1,5 s. This means that calculations using this mode of fuel modelling is still relatively computationally inexpensive.

Table 4.2. Base scenario input data values

Parameter	***Value***	***Parameter***	***Value***	***Parameter***	***Value***
R	0.02	T_∞	300	$\mu_{air,max}$	0.00004846
c_w	2300	N	200	$\mu_{air,min}$	0.00001845
c_{char}	1000	M	80	$\mu_{steam,max}$	0.0000345
l_p	-610000	m_0	0.4	$\mu_{steam,min}$	0.0000124
l_w	-2257000	σ	0.5	$\mu_{vol,max}$	0.00004125
λ_w	0.6	τ_{end}	5	$\mu_{vol,min}$	0.0000137
λ_{char}	0.1	t_{max}	2000	$k_{air,max}$	0.08236
p_0	550	u_{max}	10	$k_{air,min}$	0.02638
T_{vap}	373	Pr	0.75	$k_{vol,max}$	0.08
T_{pend}	825	g	9.81	$k_{vol,min}$	0.024
T_p	490	p_{atm}	101325	$k_{steam,max}$	0.085
$T_{max}(R)$	1300			$k_{steam,min}$	0.02457

5.1 Base Scenario Results

5.1.1. Spatiotemporal Distribution of Temperature

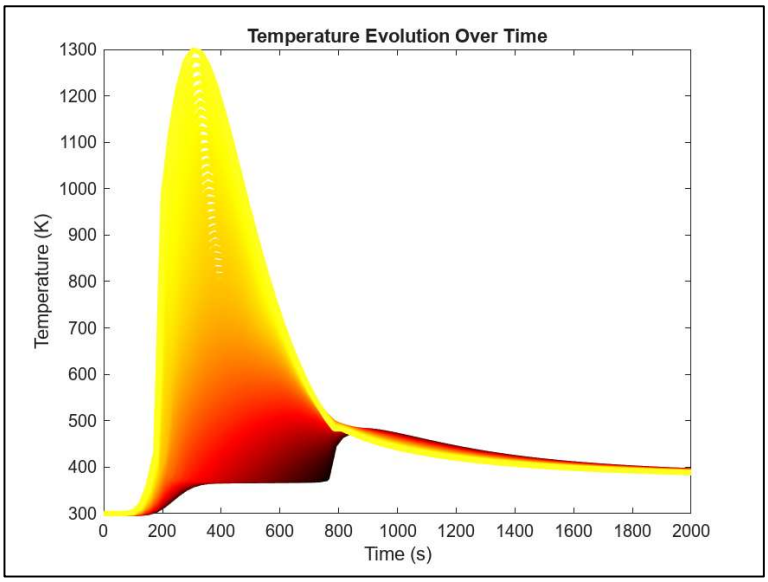

Figure 5.1. Temperature evolution of all nodes over time

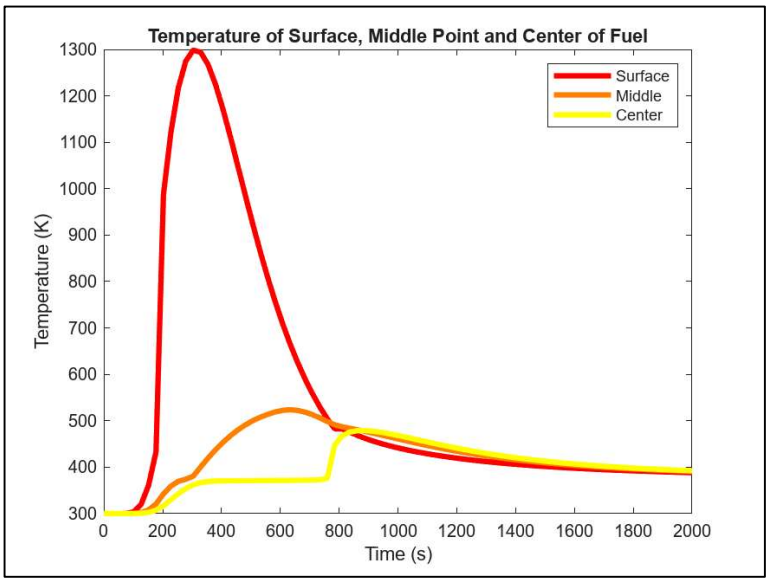

Figure 5.2. Temperature evolution of three indicative nodes, surface, center, and their middle, over time

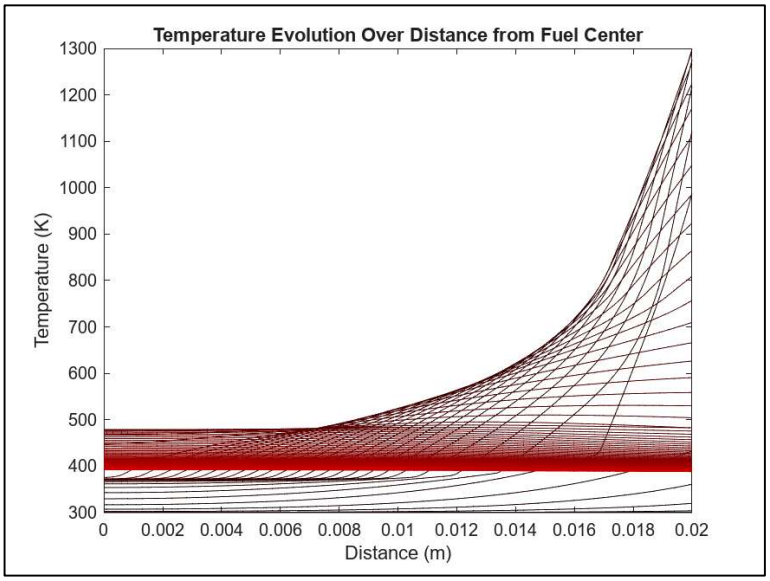

Figure 5.3. Temperature evolution over distance from particle center at all time steps

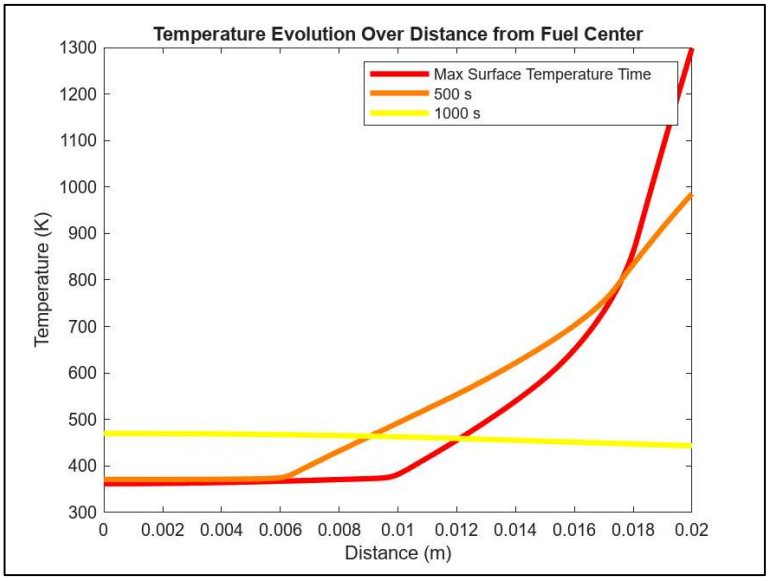

Figure 5.4. Temperature evolution over distance from fuel center for three indicative time lapses (500 s, 1000s, and time when maximum surface temperature is reached)

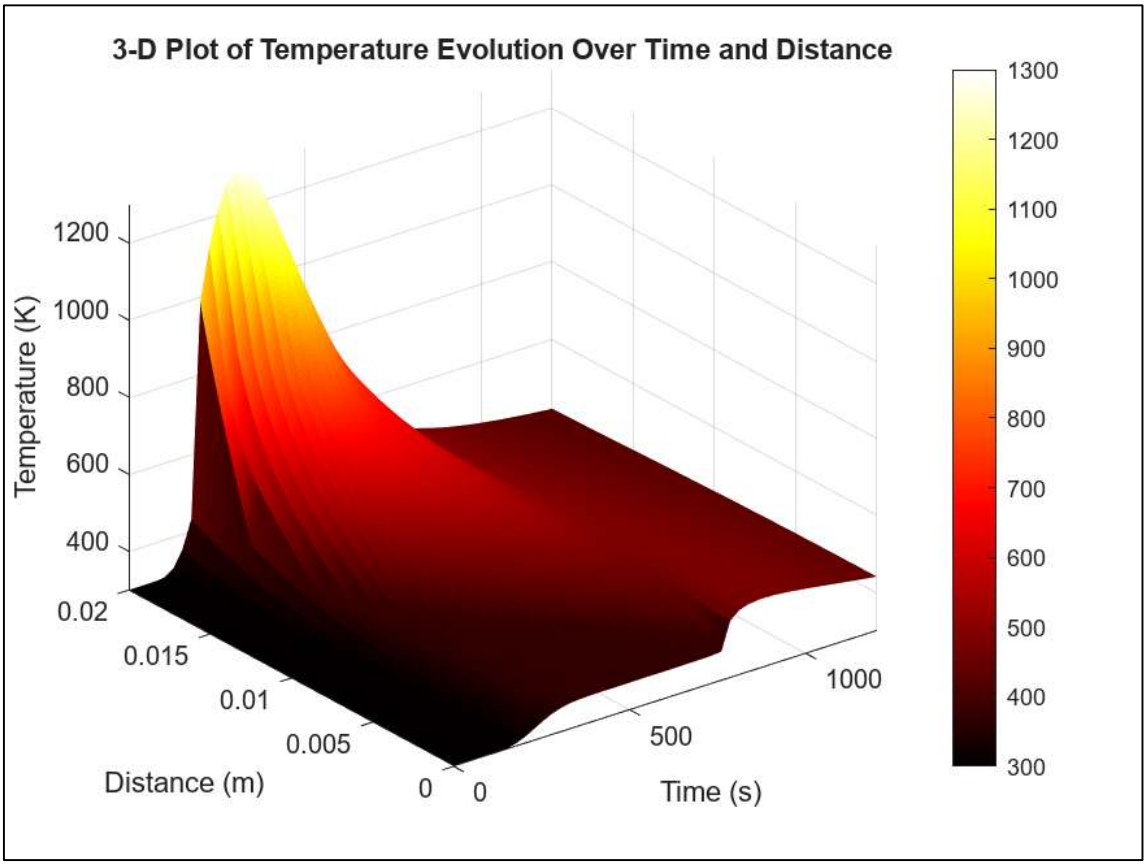

Figure 5.5. 3-D plot of temperature evolution over time and distance from fuel center

As indicated by the spatiotemporal distribution of temperature in Figures 5.1 – 5.5, the local transient temperature variation expected within a fuel's particle bulk is adequately captured by the current modelling approach and in agreement with the expected behaviour before and after the passage of the flamefront, indicated here by the curve of the surface temperature. Heat diffusion owing to the surface temperature penetrates the fuel's bulk, resulting after some point at higher temperatures deeper in the particle although the surface has already cooled down. This behaviour is consistent with phenomena such as glowing and smouldering combustion, as high temperatures may be maintained within the particle after flaming combustion driven by volatile oxidation in the particle's surface has ceased.

5.1.2. Steam and Volatile Generation

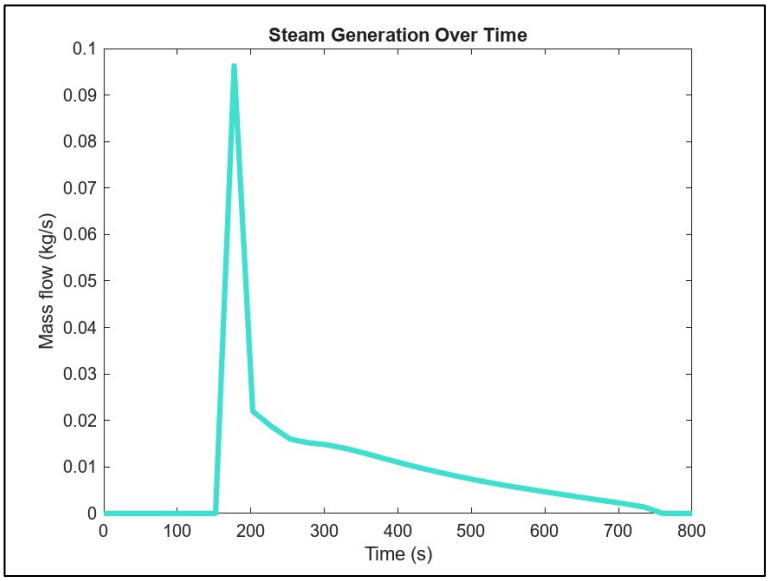

Figure 5.6. Steam generation over time

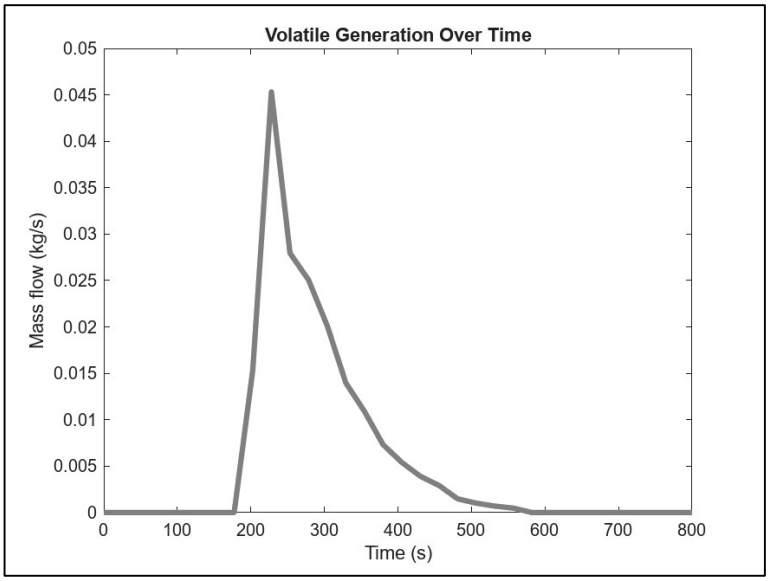

Figure 5.7. Volatile generation over time

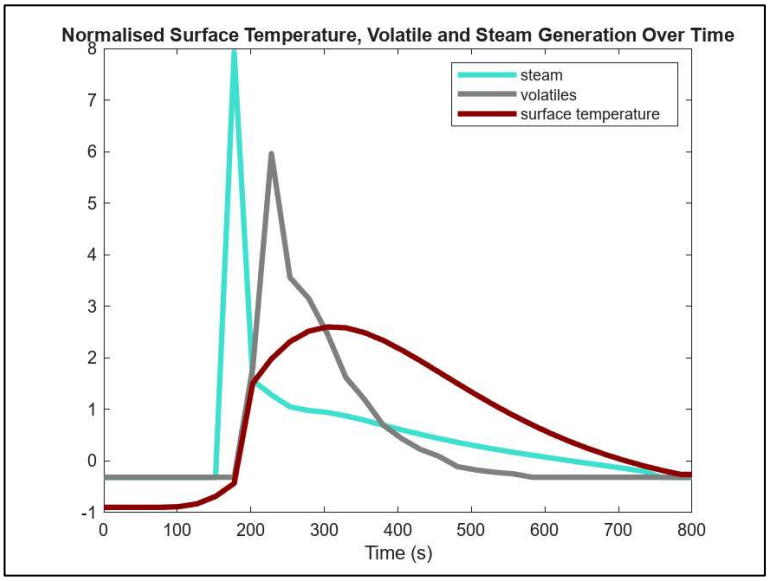

Figure 5.8. Normalised steam and volatile generation and surface maximum temperature over time

The inclusion of Figure 5.8, depicting normalized versions of steam generation, volatile generation and surface temperature over time is for exploring their potential correlation. An important first note on steam and volatile generation is that, as discussed in the previous chapter, they are explicitly determined at each time step and not a part of the implicit scheme. This creates the problem that, while the implicitly determined temperature distribution is largely independent of the time step, steam and volatile generation are not and in fact oscillate considerably when the time step is larger than the radial step. A suitable time step to diminish the phenomenon is selected here (table 4.2).

Steam generation seems to spike steeply at a relatively small time lapse when local temperatures start to reach evaporation levels, before being more smoothly distributed until dehydration of all of the moisture content is achieved. The smoother distribution probably corresponds to temperatures deeper in the fuel's bulk remaining in the zone of evaporation for a larger amount of time while not exceeding them and moving into pyrolysis area. The sudden initial spike could be explained by the large difference of the values selected for the thermal conductivity of wet wood and char and the linear relation to temperature which has been used. A more complex relationship could bear more realistic distribution results.

Volatile generation starts after the initial spike of steam generation but continues in parallel with it. This behaviour captures the effect of local transient temperature variation, keeping parts of the fuel particle in evaporation temperature zones and others in pyrolysis ones, while also since dehydration is the first process to begin, it initially acts as a thermal

buffer, delaying the start of devolatilisation. The overlap of pyrolysis and dehydration would be insignificant for smaller particles not displaying major variations in local transient temperatures. Volatile generation seems to closely follow the temperature rise and arrives at its peak when the maximum surface temperature curve starts curbing its steepness, accounting for the energy associated with devolatilisation.

5.2 Main Sensitivity Analysis Results

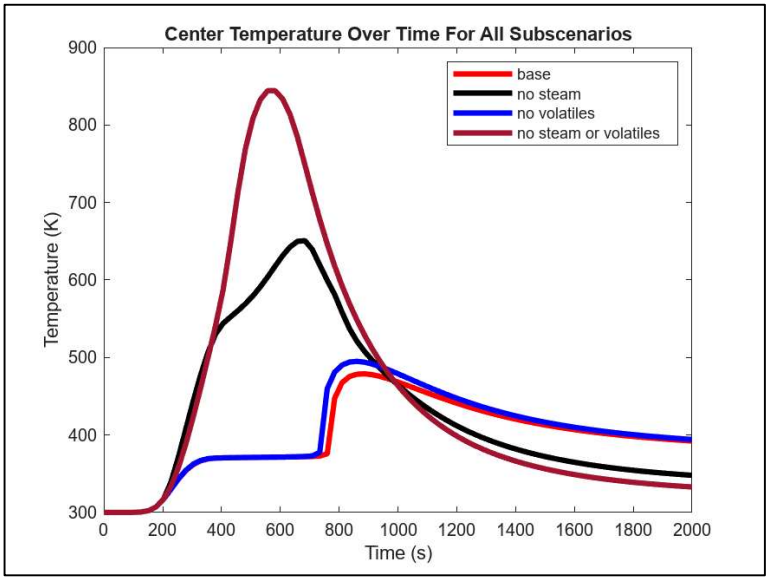

Figure 5.9. Center temperature over time for all subscenarios

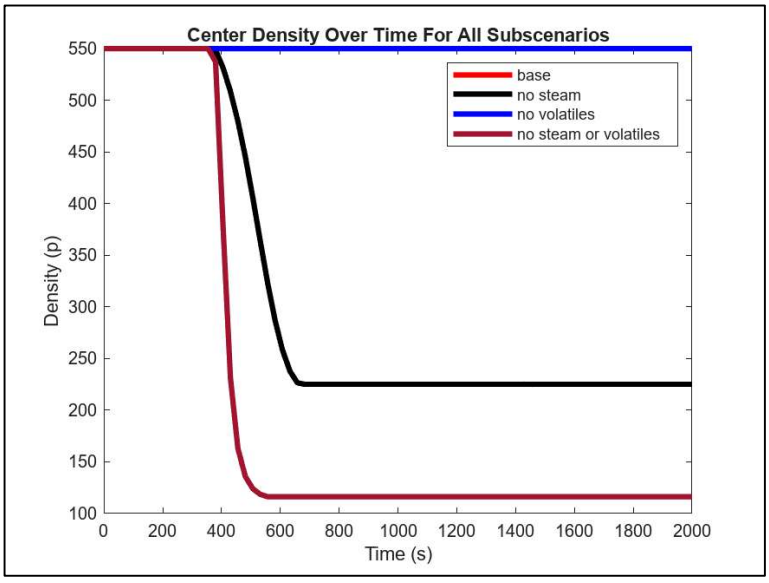

Figure 5.10. Center local density over time for all subscenarios

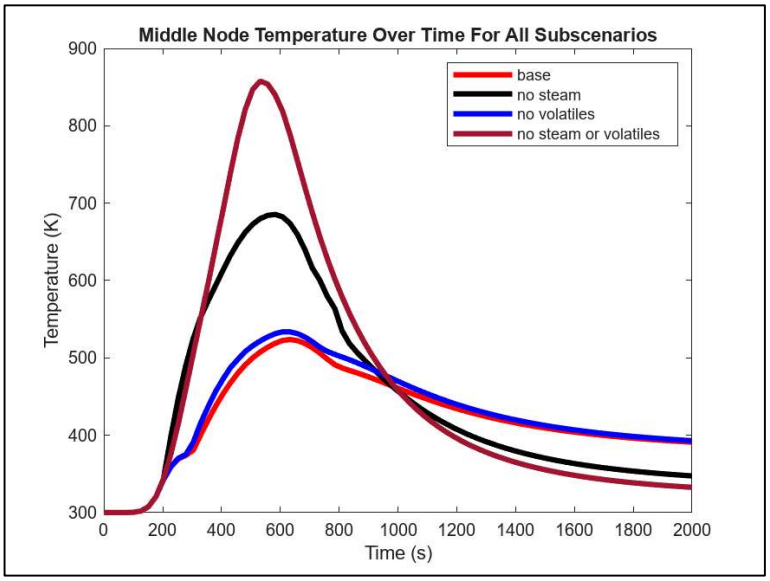

Figure 5.11. Middle node temperature over time for all subscenarios

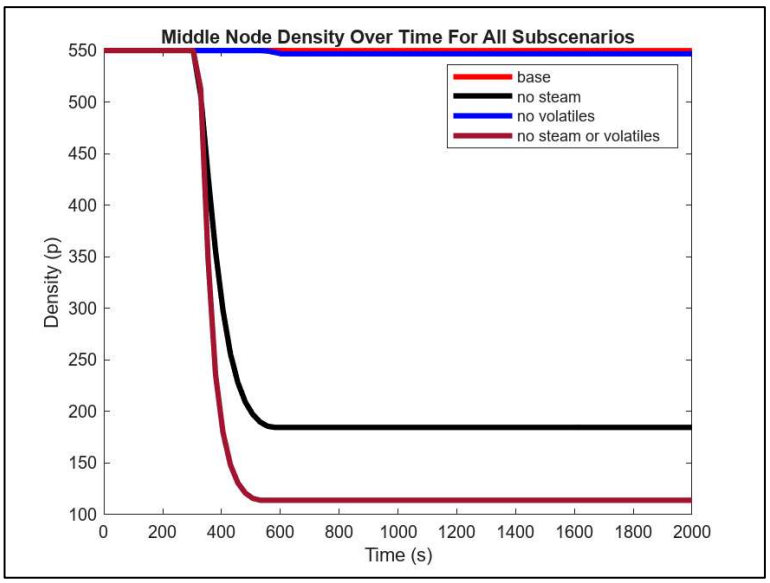

Figure 5.12. Middle node density over time for all subscenarios

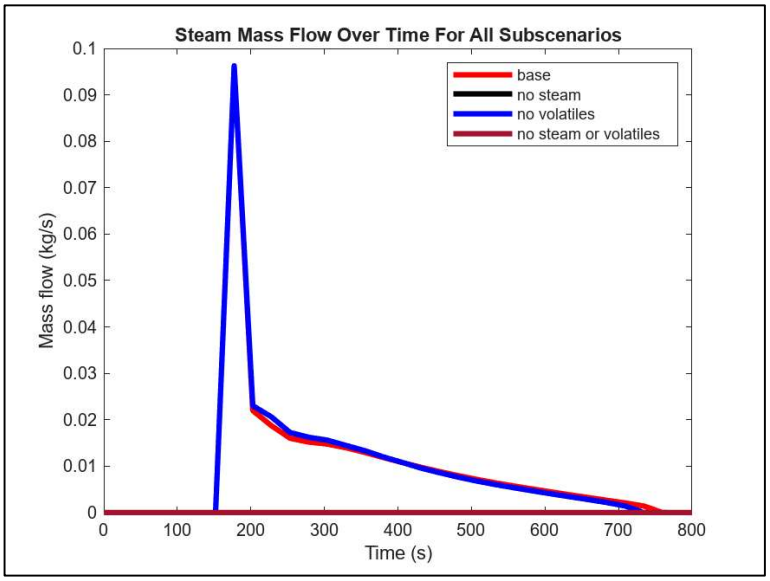

Figure 5.13. Steam mass flow over time for all subscenarios

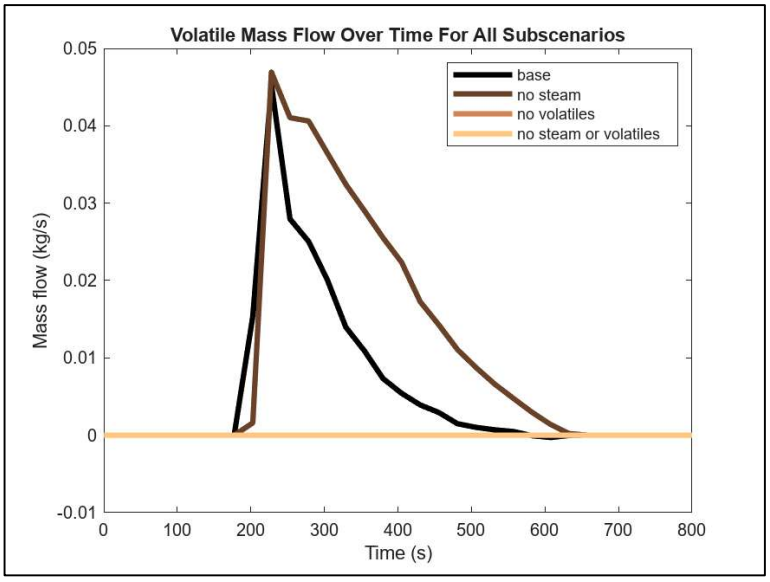

Figure 5.14. Volatile mass flow over time for all subscenarios

In the main sensitivity analysis scenario, the base scenario run results are compared to hypothetical subscenarios where no steam generation occurs (effectively the same as setting the initial moisture content as 0%), no volatile generation occurs, or neither steam nor volatile generation is taken into account. The node at the center of the fuel particle and the middle node between the particle's surface and its center are chosen as indicative nodes of the effects each subscenario assumption has on temperature and density.

The generation of steam acts as a major heat sink in the heat transfer process. This is evident by the fact that its absence, equivalent to dry wood combustion, significantly raises temperatures in the fuel's bulk, as shown in the "no steam" and "no volatiles and steam" cases, and the accompanying steep drop in local density signifies that wood is turned to char much more quickly in the absence of moisture (Figures 5.9-5.12). When examined in relation to the presence or absence of volatile generation, steam generation seems unaffected either way, as shown in Figure 5.13. The reason for this is that, since the temperature zone of it occurring is well under pyrolysis temperatures, its initialisation and finalisation is independent of it.

Disregarding volatile generation on its own does not change the temperature outcome of the base scenario by a lot, since steam generation is still acting as a heat sink. When combined with the premise of a dry wood, though, temperature rise is much quicker, denoting the absence of energy needed for thermal degradation and a direct passage to the char combustion phase. Though the opposite may not be true, volatile generation is greatly affected by the presence or absence of steam generation. As is evident in Figure 5.14 and in accordance with the findings of Saastamoinen and Richard, fuel moisture can significantly reduce the rate of devolatilisation. The absence of steam leads to much higher volatile generation rates. The reason is again the fact that dehydration begins before devolatilisation and delays temperature rising in pyrolysis temperature zones even in the case of large particles where these processes run in parallel to some degree.

5.3 Moisture Sensitivity Analysis Results

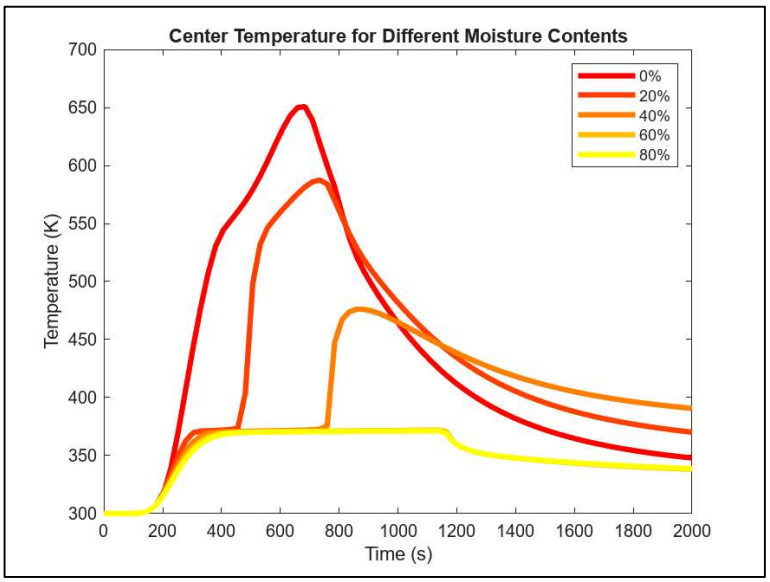

Figure 5.15. Center node temperature for different initial moisture contents

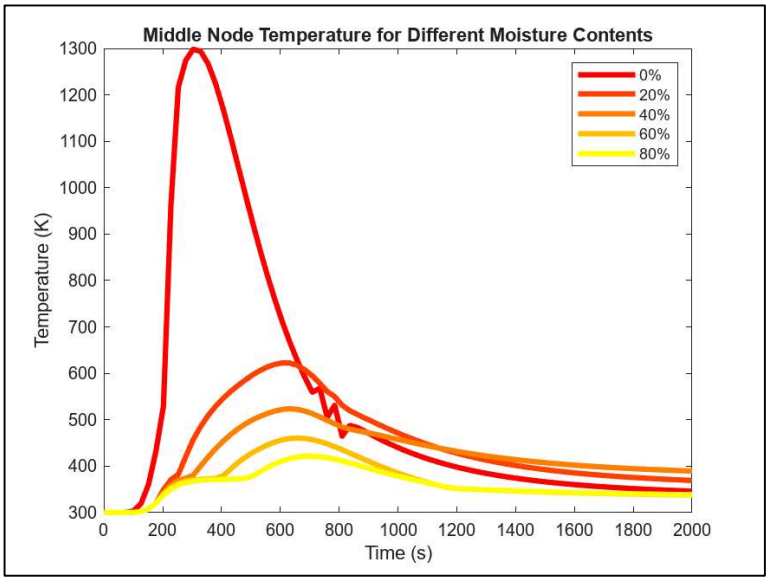

Figure 5.16. Middle node temperature for different moisture contents

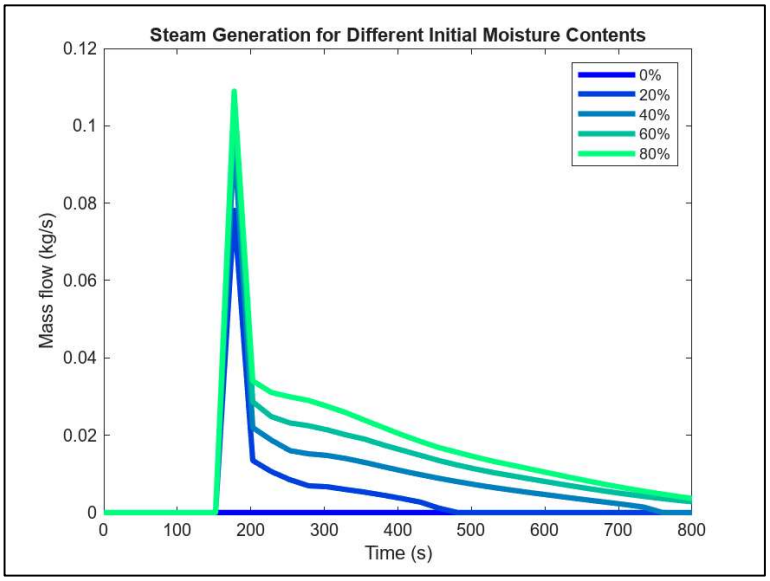

Figure 5.17. Steam generation for different initial moisture contents

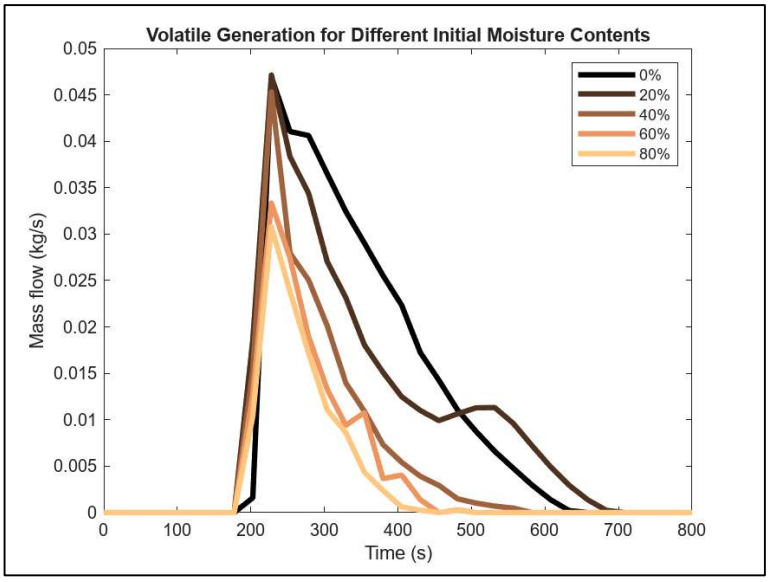

Figure 5.18. Volatile generation for different initial moisture contents

The moisture sensitivity analysis examines the effect of different initial moisture content present in the fuel particle. Center and middle nodes are again chosen as representative nodes. The results largely confirm and expand upon the findings of the main sensitivity analysis run. The absence of water content in the fuel accelerates heat transfer significantly, to the point that the middle point of the fuel can even reach the temperature of the surface. Higher contents delay heat transfer due to the energy being used for dehydration. The higher the content, the more likely it is that the fuel's bulk will never reach neither pyrolysis nor even dehydration temperatures (Figures 5.15-5.16), effectively capturing the extinguishing effect high moisture content has on fuel combustion.

Steam generation is perpetuated for longer and at higher rates past its initial peak the more moisture content there is in the initial fuel (Figure 5.17). Accordingly, volatile generation, as shown in the main sensitivity analysis, is that much more inhibited the more moisture content there needs to be evaporated.

It is important to note that despite the low time step used for these runs, the effects of the inconsistency between implicitly calculated temperature and explicitly calculated rates of steam and volatile generation shows as minor fluctuations in cases where finer calculations need to be made, like in the volatile sensitivity analysis.

5.4 Radius Sensitivity Analysis Results

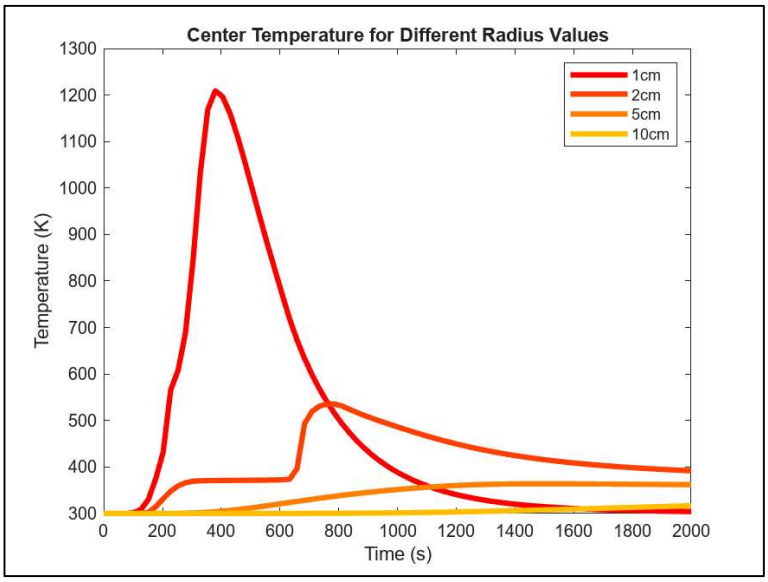

Figure 5.19. Center temperature for different radius values

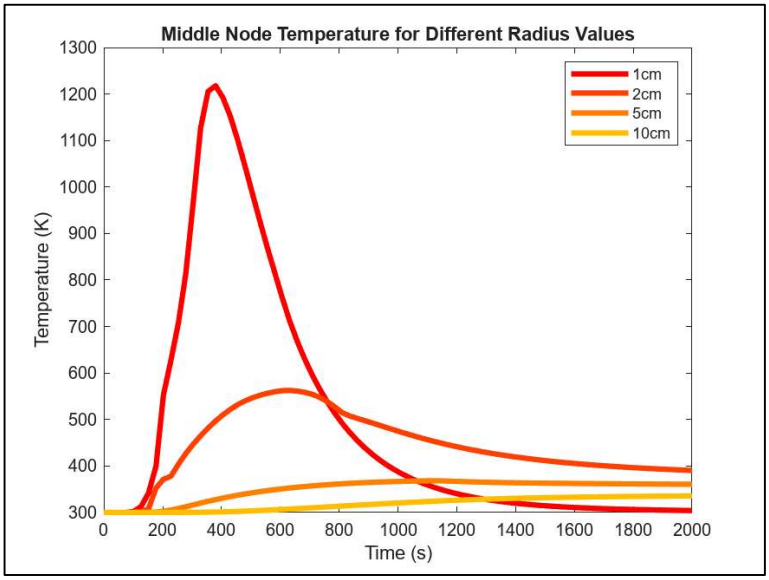

Figure 5.20. Middle node temperature for different radius sizes

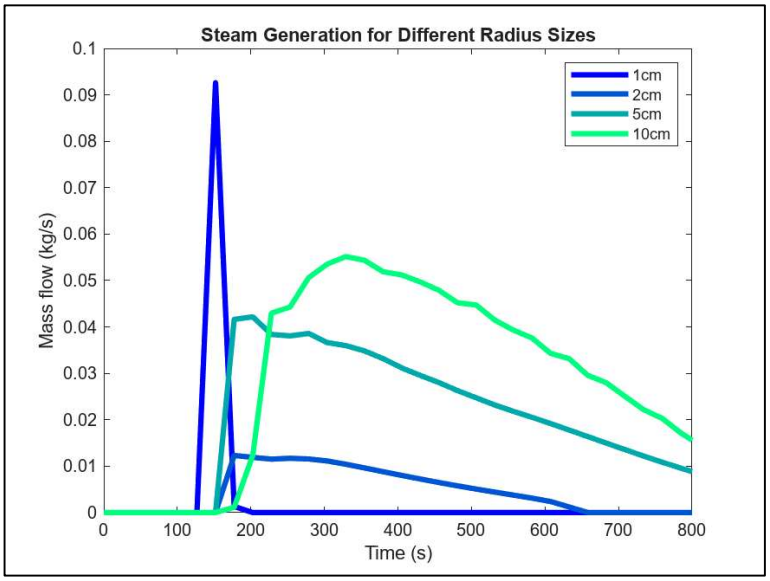

Figure 5.21. Steam generation for different radius sizes

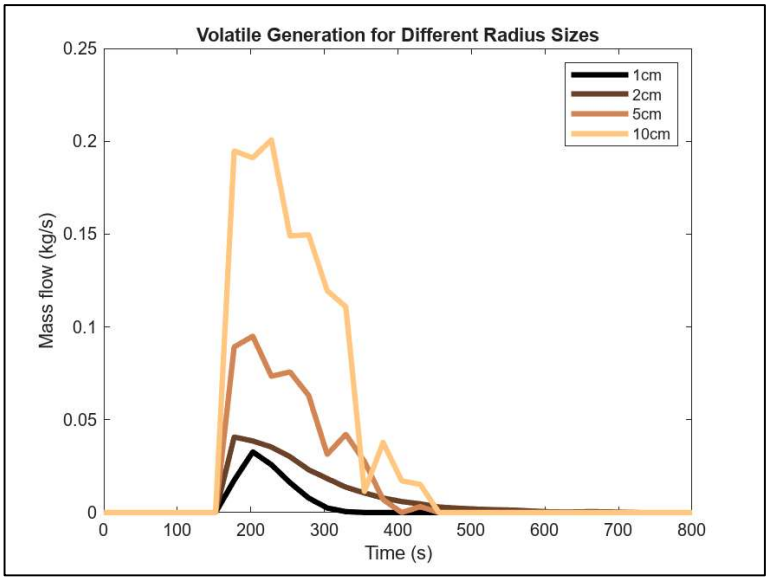

Figure 5.22. Volatile generation for different radius sizes

The final sensitivity analysis run concerns the effect of different paricle radius sizes on the results. Figures 5.19 and 5.20 show that local transient temperature variation in fuel particles of 1 cm or below has no significant effect. The middle and center nodes follow very closely the temperatures expected in the particle's surface. Higher values of radius instead expect heat transfer penetration in the fuel's bulk to be slower and less effective, with larger particles' center temperature remaining even at the base level.

Steam generation in larger particles presents a more streamlined rate for the whole of the dehydration process. Essentially, the initial pike is smoothed and slower evaporation rates are sustained, as heat transfer is more slowly reaching the fuel's bulk and evaporation temperature is sustained over a larger amount of wood mass for a longer time.

Volatile generation, on the other hand, exhibits higher rates for larger particles. This is to be expected as a larger amount of available mass is pyrolised and devolatilisation may even help sustain flaming temperatures in the surface, aiding heat transfer to the bulk and amassing even larger amounts of volatiles in a loop until charring.

The effect of the time step is again evident. Both volatile and steam generation wildly oscillate for larger particles, owning to the fact that their explicit calculations need both a small time step and a finer mesh in order to be smoothed. The chosen mesh and time step is an approximation allowing for both reasonable results but also making this disadvantage evident.

Chapter 6. Conclusion – Suggestions for Further Research

A modelling approach of fuel particle dehydration, thermal degradation and combustion based on heat transfer was developed, integrated into a MATLAB code and numerically tested. The aim was overcoming the inherent limitations of approaching these reactions with Arrhenius kinetics in the context of larger fuel particles. When used as part of larger wildfire spread models, these limitations may tend to overestimate volatile generation which is a major driver of flaming combustion and as such the rate of spread itself. The interplay and overlap between steam and volatile generation is also difficult to capture this way. Approaching the reactions as a one-dimensional heat diffusion problem accounts for the spatiotemporal variation in local transient temperature in a fuel's bulk, allowing for a more accurate representation of temperature allocation, steam and volatile generation.

The heat diffusion partial differential equation describing the process was numerically approached by a semi-implicit finite difference scheme, and various sensitivity analyses were run to explore relations between reaction components and fuel characteristics. The findings include the significant role of moisture as a heat sink and its inhibiting role on volatile generation, the fact that steam and volatile generation indeed always overlap to some degree but this overlap is insignificant in smaller particles, and the absence of a limiting case of fuel particle size when the problem is approached this way. This modelling approach can indeed capture local variations of transient temperature and its effects and is as such an adequate alternative approach to Arrhenius kinetics. This capture can also simulate effects like smouldering and glowing combustion in the fuel's bulk, something not possible when approached by the uniform fire layer temperature that Arrhenius rates imply.

A major disadvantage that if overcome could significantly improve model performance is the inconsistency between implicitly calculated temperature and explicitly calculated temperature-dependent terms. As explained in Chapter 4, while temperature is calculated using the vector of known temperatures, the terms dependent of temperature and appearing in the coefficient matrix are calculated at each time step using the current and not the next temperature. This results in instability and oscillations in the temperature dependent terms, such as steam and volatile generation, if the time and radial step aren't fine-tuned. A number of different approaches to solving this problem could be applied, such as incorporating the

term $H(T)$ in the implicit scheme, refining the grid by an adaptive mesh refinement technique or similar, or employing post-processing data smoothing techniques.

For this modelling approach, pyrolysis and combustion have been assumed to be purely heat transfer dominated reactions with very high kinetic rates. Although this could be adequate, there might be an advantage in setting a criterion for which a change from a heat transfer to a kinetic dominated process occurs, improving accuracy of steam and volatile generation calculations.

As discussed in Chapter 5, the linear approach of correlating temperature with heat conductivity may be inaccurate especially in the context of steam generation. More complex calculations have been suggested (Saastamoinen and Richard, 1996) which may again improve accuracy of calculations of derivative terms.

There are some effects which have been neglected in the current approach. The two most likely to have and actual impact is the convective cooling effect the flow of volatiles and steam may have in the direction opposite to the heat transfer. Saastamoinen and Richard for example incorporate this by substracting an integrative term from the right hand heat transfer term. Similarly, the transfer of moisture as liquid water may also be incorporated into the temperature calculation. Shrinkage or swelling effects of biomass during thermal degradation could also be taken into account.

References

Andrews, Patricia L. (2018), The Rothermel surface fire spread model and associated developments: A comprehensive explanation, *General Technical Report RMRS-GTR-371*, Fort Collins, CO: U.S. Department of Agriculture, Forest Service, Rocky Mountain Research Station, 121.
https://doi.org/10.2737/RMRS-GTR-371

Andrews, P. L. (2014), Current status and future needs of the BehavePlus Fire Modeling System, *International Journal of Wildland Fire 23*, 21-33.
https://doi.org/10.1071/WF12167

Bakhshaii, A., Johnson, E.A. (2019), A review of a new generation of wildfire–atmosphere modeling, *Canadian Journal of Forest Research 49*(6), 565-574.
https://doi.org/10.1139/cjfr-2018-0138

Bargali, H., Pandey, A., Bhatt, D., Sundriyal, R.C., Uniyal, V.P. (2024), Forest fire management, funding dynamics, and research in the burning frontier: A comprehensive review, *Trees, Forests and People 16*.
https://doi.org/10.1016/j.tfp.2024.100526

Cengel, Y.A. (2002), Heat Transfer: A Practical Approach, 2nd Edition, McGraw-Hill, New York.

Cunningham, C.X., Williamson, G.J. & Bowman, D.M.J.S. (2024), Increasing frequency and intensity of the most extreme wildfires on Earth, *Nat Ecol Evol 8*, 1420–1425.
https://doi.org/10.1038/s41559-024-02452-2

Duane, A., Castellnou, M. & Brotons, L. (2021), Towards a comprehensive look at global drivers of novel extreme wildfire events, *Climatic Change 165*, 43.
https://doi.org/10.1007/s10584-021-03066-4

Jain, P., Coogan S.C.P., Subramanian S.G., Crowley M, Taylor, S., & Flannigan, M.D.(2020), A review of machine learning applications in wildfire science and management, Environmental Reviews 28(4), 478-505.
https://doi.org/10.1139/er-2020-0019

Kala, C.P. (2023), Environmental and socioeconomic impacts of forest fires: A call for multilateral cooperation and management interventions, *Natural Hazards Research 3*(2), 286-294.
https://doi.org/10.1016/j.nhres.2023.04.003

Leckner, B., Hansson, K.M., Tullin, C., Borodulya, A.V., Dikalenko, V. I.; Palchonok, G. I. (199), Kinetics of fluidized bed combustion of wood pellets, 15th International Conference on Fluidized Bed Combustion, Savannah, GA (US).

Mandel, J., Bennethum, L.S., Beezley, J.D., Coen, J.L., Douglas, C.C., Kim, M., Vodacek, A. (2008), A wildland fire model with data assimilation, *Mathematics and Computers in Simulation 79*(3), 584-606.
https://doi.org/10.1016/j.matcom.2008.03.015

McNorton, J. R. and Di Giuseppe, F. (2024), A global fuel characteristic model and dataset for wildfire prediction, *Biogeosciences 21*, 279–300.
https://doi.org/10.5194/bg-21-279-2024, 2024.

Mhawej, M., Faour, G., & Adjizian-Gerard, J. (2015), Wildfire Likelihood's Elements: A Literature Review, *Challenges 6*(2), 282-293.
https://doi.org/10.3390/challe6020282

Mueller, S.E., Thode, A.E., Margolis, E.Q., Yocom, L.L., Young, J.D., Iniguez, J.M. (2020), Climate relationships with increasing wildfire in the southwestern US from 1984 to 2015, *Forest Ecology and Management 460*.
https://doi.org/10.1016/j.foreco.2019.117861

Naian, L., Jiao, L., Wei, G., Haixiang, C., Xiaodong, X. (2021), Combustion dynamics of large-scale wildfires, *Proceedings of the Combustion Institute 38*(1), 157-198
https://doi.org/10.1016/j.proci.2020.11.006

Nunes, A.N., Lourenço, L., Castro Meira, A.C. (2016), Exploring spatial patterns and drivers of forest fires in Portugal (1980–2014), *Science of The Total Environment 573*, 1190-1202. https://doi.org/10.1016/j.scitotenv.2016.03.121

Pastor, E., Zárate, L., Planas, E., Arnaldos, J. (2003), Mathematical models and calculation systems for the study of wildland fire behaviour, *Progress in Energy and Combustion Science 29*(2), 139-153.
https://doi.org/10.1016/S0360-1285(03)00017-0

Porteiro, J., Míguez, J.L., Granada, E., Moran, J.C. (2006), Mathematical modelling of the combustion of a single wood particle, *Fuel Processing Technology 87*(2), 169-175.
https://doi.org/10.1016/j.fuproc.2005.08.012

Ragland, K.W., Aerts, D.J., Baker, A.J. (1991), Properties of wood for combustion analysis, *Bioresource Technology 37*(2), 161-168.
https://doi.org/10.1016/0960-8524(91)90205-X

Rein, G. (2013), Smouldering Fires and Natural Fuels, in: *Fire Phenomena and the Earth System: An Interdisciplinary Guide to Fire Science*, Belcher, C. (ed.), Wiley and Sons, 15–33.
https://doi.org/10.1002/9781118529539.ch2

Román, M.V., Azqueta, D., Rodrígues, M. (2013), Methodological approach to assess the socio-economic vulnerability to wildfires in Spain, *Forest Ecology and Management 294*, 158-165.
https://doi.org/10.1016/j.foreco.2012.07.001

Saastamoinen, J., Richard, J.R. (1996), Simultaneous drying and pyrolysis of solid fuel particles, *Combustion and Flame 106* (3), 288-300
https://doi.org/10.1016/0010-2180(96)00001-6

Singh, H., Ang, LM., Lewis, T. et al. (2024), Trending and emerging prospects of physics-based and ML-based wildfire spread models: a comprehensive review, *Journal of Forestry Research 35*, 135.
https://doi.org/10.1007/s11676-024-01783-x

Sullivan, A. L. (2009), Wildland surface fire spread modelling, 1990–2007. 1: Physical and quasi-physical models. *International Journal of Wildland Fire*, *18*(4), 349-368.
https://doi.org/10.1071/WF06143

Sullivan, A.L. (2022), Wildland Fire Combustion Dynamics: The Intersection of Combustion Chemistry and Fluid Dynamics, in: *Wildland Fire Dynamics,* Cambridge: Cambridge University Press, K. Speer and S. Goodrick (eds.) , 1–34.
https://doi.org/10.1017/9781108683241.001

Sutanto, S. J., Janssen, M., de Brito, M. M., del Pozo Garcia, M. (2024), The effect of wildfires on flood risk: a multi-hazard flood risk approach for the Ebro River basin, Spain, *Natural Hazards Earth System Sciences 24,* 3703–3721.
https://doi.org/10.5194/nhess-24-3703-2024

Weber, R.O. (1991), Modelling fire spread through fuel beds, *Progress in Energy and Combustion Science 17*(1), 67-82.
https://doi.org/10.1016/0360-1285(91)90003-6

Wells, G. (2008), The Rothermel Fire-Spread Model: Still Running Like a Champ, *Joint Fire Science Program Digests 2*.
https://digitalcommons.unl.edu/jfspdigest/2

Zacharakis, I., Tsihrintzis, V. A. (2023), Environmental Forest Fire Danger Rating Systems and Indices around the Globe: A Review. *Land*, *12*(1), 194.
https://doi.org/10.3390/land12010194